buildings

MDPI

Review

A Review on Damage Monitoring and Identification Methods for Arch Bridges

Jiafeng Yang [1,2], Lei Huang [3], Kai Tong [3], Qizhi Tang [3], Houxuan Li [3], Haonan Cai [3] and Jingzhou Xin [4,*]

1 School of Civil Engineering, Central South University, Changsha 410075, China; ctjtyjf@126.com
2 Chongqing Railway Investment Group Co., Ltd., Chongqing 400023, China
3 School of Civil Engineering, Chongqing Jiaotong University, Chongqing 400074, China; huanglei@mails.cqjtu.edu.cn (L.H.); kaitong@mails.cqjtu.edu.cn (K.T.); tangqizhi1015@163.com (Q.T.); hxli@mails.cqjtu.edu.cn (H.L.); 611210080005@mails.cqjtu.edu.cn (H.C.)
4 State Key Laboratory of Mountain Bridges and Tunnel Engineering, Chongqing Jiaotong University, Chongqing 400074, China
* Correspondence: xinjz@cqjtu.edu.cn

Abstract: The damage monitoring and identification of arch bridges provide an important means to ensure the safe operation of arch bridges. At present, many methods have been developed, and the applicability and effectiveness of these methods depend on the damage type, structural configuration and available data. To guide the practical application of these methods, a systematic review is implemented in this paper. Specifically, the damage monitoring and identification methods of arch bridges are divided into the damage monitoring of local diseases and damage identification of overall performance. Firstly, the research on the damage monitoring of the local diseases of arch bridges is reviewed. According to the disease type, it is divided into four categories, including suspender inspection, void monitoring, stress detection and corrosion detection. For each disease, this paper analyzes the principles, advantages and shortcomings of various methods. Then, the damage identification methods of the overall performance of arch bridges are reviewed, including masonry arch bridges, steel arch bridges, reinforced concrete arch bridges and concrete-filled steel tubular arch bridges. And the commonly used damage indexes of damage identification methods are summarized. This review aims to help researchers and practitioners in implementing existing damage detection methods effectively and developing more reliable and practical methods for arch bridges in the future.

Keywords: arch bridge; damage monitoring; damage identification

Citation: Yang, J.; Huang, L.; Tong, K.; Tang, Q.; Li, H.; Cai, H.; Xin, J. A Review on Damage Monitoring and Identification Methods for Arch Bridges. *Buildings* **2023**, *13*, 1975. https://doi.org/10.3390/buildings13081975

Academic Editor: Weixin Ren

Received: 29 June 2023
Revised: 25 July 2023
Accepted: 28 July 2023
Published: 2 August 2023

1. Introduction

Arch bridges have been widely used in transportation infrastructure construction because of their large structural stiffness, affordability and strong adaptability in mountainous areas. However, under the coupling effect of an external complex environment and internal material degradation, arch bridges inevitably face the risk of performance degradation [1–4], resulting in different degrees of damage to the structure. These damages will reduce the bearing capacity and service life of the arch bridge and even endanger the safety of the bridge. An unpredicted structural failure can be catastrophic not only in terms of life and economic losses but also in terms of the subsequent societal impacts [5]. Therefore, monitoring and identifying the damage state of the arch bridge in a timely manner can improve the structural safety and reduce the later maintenance cost, which is of great significance for ensuring the normal operation of the arch bridge and prolonging its service life.

Structural damage identification methods can be divided into two categories: local damage identification and overall damage identification [5]. The local damage monitoring method uses advanced sensors, non-destructive testing and other means to directly

diagnose the local damage status of the structure. By contrast, the overall damage identification method uses data mining of structural response information to indirectly extract the characterization index of the structural damage status [6–12]. As a large and complex civil structure, arch bridges have many key components, and the damage monitoring and identification methods of arch bridges are complicated. In order to make research on the damage identification of arch bridges more systematic, this paper makes a clear classification of the existing methods, which is more practical and comprehensive. Considering the specific structural characteristics of a bridge, the existing methods are classified and then reviewed. Specifically, the damage monitoring and identification methods of arch bridges are divided into two categories: damage monitoring methods for local diseases of arch bridges and damage identification methods for the overall performance of arch bridges. The former mainly focuses on the detailed detection of a certain part or a component of the arch bridge structure, such as suspenders, arch rings, joints, etc., to find out whether there are local diseases such as corrosion, cracks and fractures; the latter mainly analyzes the overall response of the arch bridge structure, such as frequency, mode, stiffness, etc., to determine whether there is a global damage such as overall performance degradation or structural deformation.

Section 2 summarizes the damage monitoring for local diseases of arch bridges, including suspender inspection, void monitoring, stress detection and corrosion detection. In Section 3, the damage identification of the overall performance of arch bridges is described in detail. According to the development history of an arch bridge and the different construction materials used, it is divided into the following four types: masonry arch bridge, steel arch bridge, reinforced concrete (RC) arch bridge and concrete-filled steel tube (CFST) arch bridge.

2. Damage Monitoring for Local Diseases of Arch Bridge

The damage monitoring of local diseases for arch bridges is mainly realized by physical means, such as the ultrasonic method, magnetic memory method, thermal imaging method, etc. Considering the key bearing member, common disease problems and important safety performance indicators of various types of arch bridges, this paper divides the damage monitoring of local diseases into the following four categories: suspender inspection, void monitoring, stress detection and corrosion detection. Different structural objects and different diseases have their own detection methods. The following summarizes these methods, clarifies their detection principles, compares their advantages and shortcomings, and concludes the development status of each method.

2.1. Suspender Inspection

Among many types of arch bridges, a tied arch bridge is a special bridge type that combines the advantages of arch and beam. It supports the bridge deck load by the cables suspended at the top of the main arch, thereby reducing the span and height of the main arch and making the bridge light, economical and aesthetic [13]. The cable is the key bearing member of this kind of bridge to transmit the dead load and live load. It is composed of internal stress steel wires, an anchorage system and an external protection system (high-density polyethylene (HDPE) material sheath) (as shown in Figure 1). However, subjected to the bridge dead load, vehicles, wind and temperature, the protection system of the cable is prone to damage, which makes the internal steel wire of the cable rust or even break, seriously affecting the safety of the whole bridge [14]. In addition, because the cable is high above the ground, and the outer surface of the cable is wrapped by the HDPE protective sleeve, the damage of the cable is concealed and difficult to detect and prevent. The detection of the cable has attracted extensive attention from researchers [15–17]. With the development of non-destructive techniques, a variety of innovative detection methods based on acoustics, magnetism, electricity and machine vision have emerged in the detection of arch bridge cables.

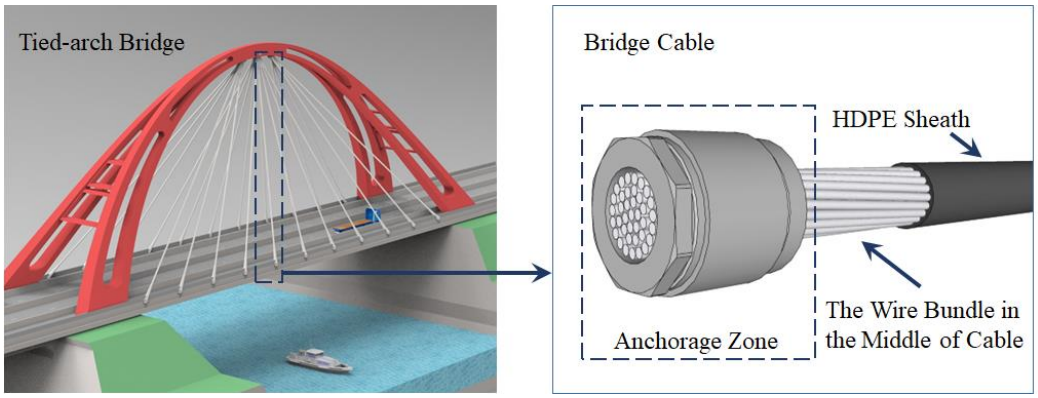

Figure 1. Cable structure diagram of tied arch bridge.

Acoustic emission testing (AET), as a long-developed non-destructive technique, has been widely used in the detection of suspenders. Its principle is to judge whether there are cracks or fractures inside the suspenders by analyzing the characteristics of acoustic signals. To reduce the influence of the environment on the detection effect, Zhu et al. [18] clarified the influence of the stress state of the suspender, the position of the measuring point, and the HDPE sheath on the AET effect and used AET to accurately determine the location of the suspender fracture. On this basis, Djeddi et al. [19] used AET to monitor the cracking process of the cable under the stress–corrosion coupling state, which filled the gap of acoustic emission in the suspender corrosion detection field. Some researchers also used AET for damage detection inside the suspender anchor head [20]. Sun et al. [21] determined the location and generation time of fatigue cracks in the steel wire inside the anchor head by analyzing the variation law of fatigue crack acoustic signals. The detection principle can be found in Figure 2. In addition, Kharrat and Gaillet [22] innovatively combined the acoustic emission principle with ultrasonic technology to realize the detection and classification of different damage degrees of anchor head.

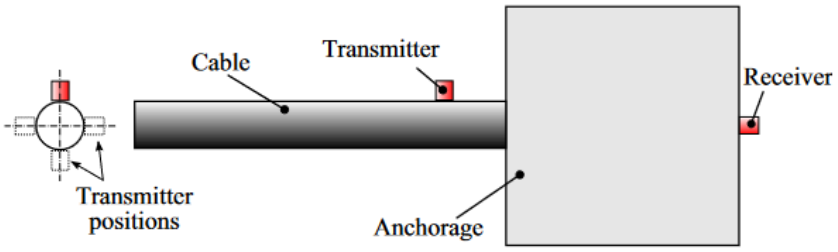

Figure 2. The principle of acoustic emission and the principle of ultrasonic technology to detect the damage of anchorage zone [21].

Magnetostrictive guided wave technology is a high sensitivity method for detecting broken wires of suspenders. The principle is that when the magnetic field induction coil generates an alternating magnetic field, a specific reflection signal will be generated at the damage of the suspender based on the magnetostrictive effect, which is converted into the information of the internal defects or damage of the suspender by signal processing technology (as shown in Figure 3). In the case of a broken wire in the suspender, Xu et al. [23] provided a method combining low-frequency wave detection and high-frequency wave detection, which can simultaneously determine the broken wire defects at different locations. In order to quantify the length of the broken wire, Chen et al. [24] studied the attenuation characteristics of the low-frequency longitudinal guided wave generated by the magnetostrictive sensor in the cable theoretically and experimentally and proposed an energy-based model, which can predict the energy attenuation well. Zhang et al. [25] designed a ring permanent-magnet-biased magnetostrictive longitudinal guided wave transducer, which improved the energy

conversion efficiency of large-diameter bridge cable and promoted the practical engineering application of magnetostrictive guided wave technology.

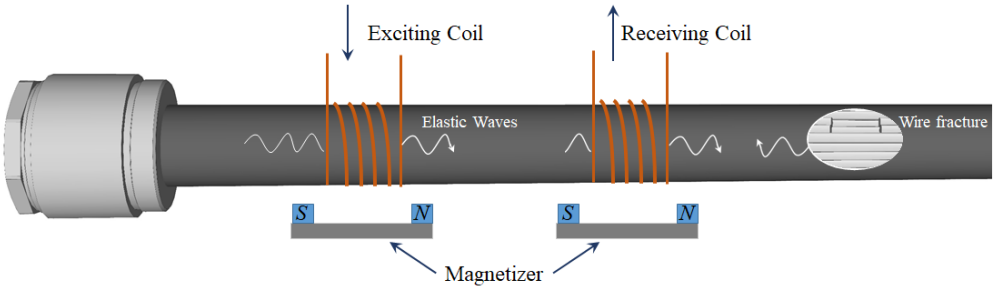

Figure 3. Magnetostrictive guided wave detection of steel wire fracture principle diagram.

Because the arch bridge suspender uses steel, which is a magnetic material, as the base material, magnetic flux leakage detection technology has also been widely used in suspender damage detection. When there are corrosion, cracks and broken wires in the suspender, the magnetic field probe (usually the Hall element) will detect the magnetic flux leakage signal on the surface of the suspender. By analyzing these magnetic flux leakage signals, the damage location and size inside the suspender can be determined (as shown in Figure 4).

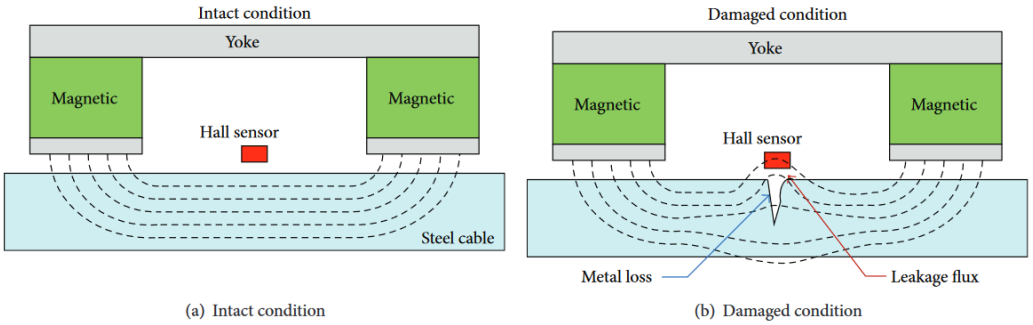

Figure 4. Principle of magnetic flux leakage detection technology [26].

At present, scholars have determined the fracture location of the steel wire inside the cable using magnetic flux leakage detection technology. However, quantifying the damage length has always been a research focus, along with the difficulty of magnetic flux leakage detection. Zhang and Xin [27] proposed an analysis model to quantify the influence of defect length, studied the influence of defect length for a magnetic flux leakage signal and verified the correctness of the model during experiments. Ni et al. [28] explored the influence of the suspender cross-section loss rate on the magnetic signal and the proposed defect length coefficient to correct the magnetic flux signal and improved the quantitative identification accuracy of the corrosion damage. To promote the practical engineering application of magnetic flux leakage detection technology, Xu et al. [29] developed the suspender climbing detection robot. The magnetic flux leakage detection system was used to detect the state of the suspender, and the filtering algorithm was used to reduce the interference signal of the environment.

The above method needs to magnetize the suspender via a strong magnetic field. The magnetization process requires heavy magnetization equipment (as shown in Figure 5), and the detection process is relatively complex [30]. Based on the principle of magnetic flux leakage detection technology, some scholars combine metal magnetic memory technology instead of artificial magnetic field excitation and analyze the magnetic flux leakage signal of suspender damage under the action of a geomagnetic field. This method has the advantages of simple operation, low cost and high efficiency [31]. In terms of suspender fracture damage detection, Qu et al. [32] proposed a cable circumferential broken wire damage

detection method based on spontaneous magnetic flux leakage, which made up for the deficiency of the circumferential detection corrosion method along the suspender. In terms of suspender corrosion detection, Xia et al. [33] proposed a probabilistic evaluation method of the suspender corrosion degree based on a Bayesian model and proposed the evaluation standard of the suspender corrosion degree based on metal magnetic memory technology for the first time. In order to explore the influence of suspender stress on this method, Xia et al. [34] carried out corrosion detection on steel strand samples under different stress states and proposed a dimensionless index, X, for the quantitative detection of corrosion.

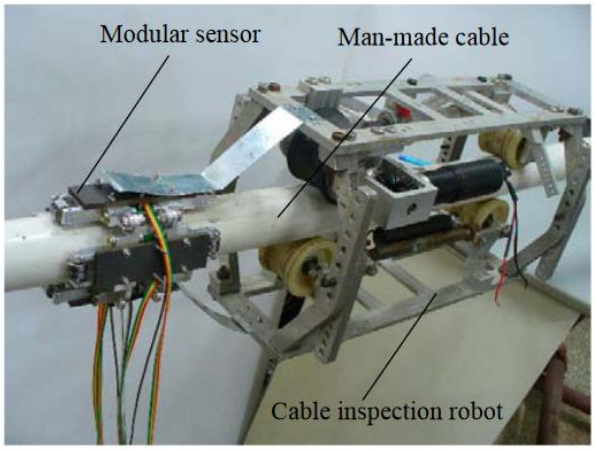

Figure 5. Suspender inspection robot based on magnetic flux leakage detection technology [30].

In recent years, piezoelectric sensors have received extensive attention from researchers due to their high sensitivity and long service life. Their principle is that the piezoelectric effect of crystals (such as quartz, strontium titanate, etc.) can be used to measure the strain of the suspender, and the anchoring efficiency of the suspender can be inferred via the relationship between stress and strain. As shown in Figure 6, Nguyen et al. [35] used the impedance-based damage estimation model to quantify the damage of the anchorage zone. The feasibility of the method was verified by the cable model experiment in the laboratory. Zhang et al. [36] monitored the loosening state of the wedge anchorage system based on the time reversal data of the sensor and proposed a method for detecting the anchoring efficiency of the suspender by using the patch piezoelectric sensor. This detection technique is the only method retrieved in this paper that can monitor the anchorage efficiency of the anchorage system.

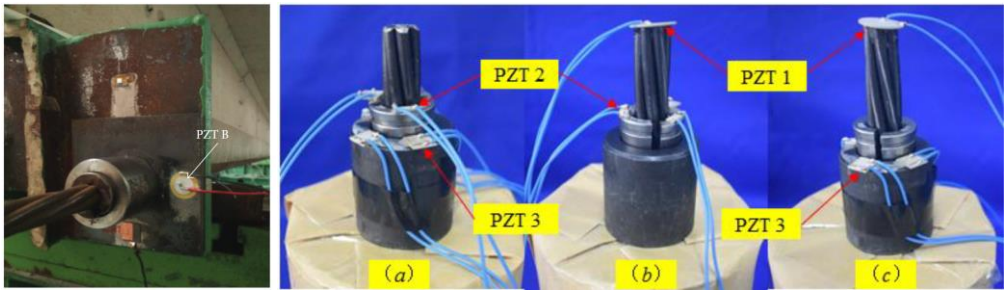

Figure 6. Piezoelectric sensor arrangement method for detecting the anchoring efficiency of suspenders: (a) contact surface between the wedge and barrel; (b) contact surface between the steel strand and wedge; (c) contact surface between the steel strand and barrel [35,36].

With the continuous development of machine vision technology, scholars have begun to use machine vision technology to detect the damage of an HDPE sheath on the surface of the suspender. This method first uses the camera or other image acquisition equipment to obtain the image or video of the suspender and then preprocesses the collected image,

including image denoising, image enhancement, edge detection and other operations, to improve the quality and clarity of the image. Finally, the machine learning algorithm is used to classify and identify the damage features, thereby realizing the automatic damage detection of the HDPE sheath. Under the influence of wind or rain flow, the suspension cables of the arch bridge may suffer from vibrations. To reduce these vibrations, the surface of the suspension cables is equipped with an HDPE protective sheath designed with indentations or protruding axials. However, this design interferes with the effectiveness of machine vision inspection. To realize image acquisition, Ho et al. [37] developed a cable-climbing detection robot. The image enhancement technology was combined with the principal component analysis (PCA) algorithm to improve the overall quality of the image collected by the robot. The length of the damage crack and the aging damage was determined by the Mahalanobis square distance (as shown in Figure 7). Hou et al. [38] proposed a transfer learning method based on the cascaded mask region-based convolutional neural network (RCNN) model for the automatic detection of surface defects of suspenders and compared it with other algorithms via field tests. It is found that this method improves the detection accuracy. Due to the different view of each camera, a single image may only collect a part of the entire defect. In order to solve this problem, Li et al. [39] proposed an efficient scale invariant feature transform (SIFT) algorithm, which realized the multi-image stitching of partially overlapping regions in different defect images and provided ideas for the all-round detection of suspenders.

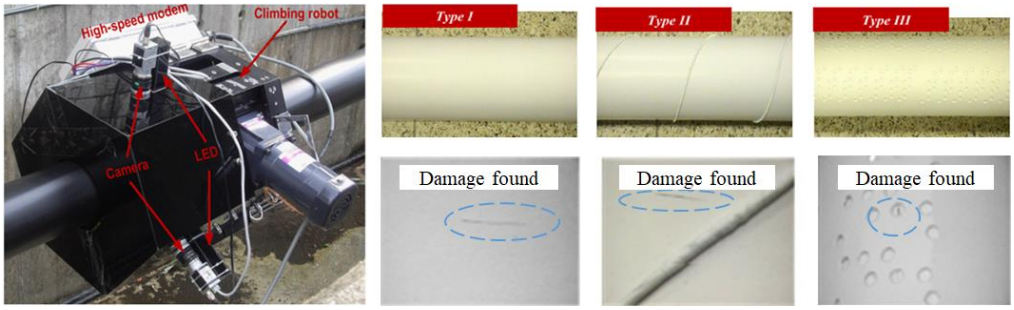

Figure 7. Climbing robot and the damage detection under three suspender surface types [37].

For the damage of an arch bridge, such as the cracking or aging of a suspender HDPE sheath, steel wire corrosion, steel wire crack or fracture, and anchorage efficiency decline, this paper summarizes the advantages, shortcomings and application scope of various detection methods, as shown in Table 1.

Table 1. Advantages and shortcomings of various detection methods for arch bridge suspenders.

Damaged Parts of Suspenders	Damage Type	Method	Advantages	Shortcomings	References
HDPE Sheath	Cracks or aging	Machine vision	The crack or aging damage of the HDPE sheath can be accurately located, and the length, width and area of the damage can be quantitatively measured.	In the early stage, a great amount of time is needed to train and debug the model. The detection effect is limited by the quality and quantity of the data set. It is impossible to judge whether the crack has penetrated into the internal steel wire.	[37–39]

Table 1. *Cont.*

Damaged Parts of Suspenders	Damage Type	Method	Advantages	Shortcomings	References
Internal steel wire of cable	Corrosion	Magnetic flux leakage testing	The quantitative measurement of the corrosion state can be realized.	The detection sensitivity of initial corrosion is poor.	[33,34]
	Fracture or crack	Acoustic emission technique	It has high sensitivity and high precision for the detection of steel wire fracture or crack position inside the suspender.	Due to the influence of the HDPE sheath, suspender length and the external HDPE sheath, the quantitative measurement of fracture length and fracture number cannot be realized, and the large area corrosion damage cannot be detected.	[18,19]
		Magnetostrictive guided wave detection technology	The testing equipment is portable and can quantitatively detect the fracture length of the internal steel wire.	The test results are affected by the length of the suspender.	[23–25]
		Magnetic flux leakage testing	The accurate positioning of steel wire fracture position and the quantitative measurement of fracture length and fracture number can be realized.	Affected by the environmental magnetic field, it is not sensitive to closed cracks.	[27–29,32]
Anchorage system	Anchoring efficiency decreased	Piezoelectric transducer	The detection cost is low. This is the only method that can monitor the anchorage efficiency of the anchorage system found in this paper.	Some sensors need to be moisture-proof, the output signal is weak, and sensors need to be deployed during the bridge construction period. There is no practical application yet.	[35,36]

2.2. Void Monitoring

The cooperative work of a steel tube and concrete is the key to ensure the bearing capacity of a CFST arch bridge [40,41]. Due to the load, temperature stress, creep shrinkage and construction stage bubble aggregation, among other reasons, the CFST arch bridge often suffers void disease. At present, many nondestructive means have been used in the void detection of a CFST, such as the ultrasonic method [42], impact–echo method [43], optical fiber sensor method [44,45] and infrared thermal imaging method [46].

Ultrasonic detection detects interface changes by detecting echo signals to achieve void detection. Researchers use the velocity of ultrasonic waves in different media to evaluate the defects of a CFST [47,48]. For example, Dong et al. [49] studied the motion path of ultrasonic waves in a CFST with void disease. Callejas et al. [50] showed that broadband ultrasound attenuation (BUA) has a linear relationship with the percentage of air in a CFST via experimental research. The void in a CFST can be detected effectively via BUA. Liu et al. [51] proposed an ultrasonic detection method for voids in CFSTs by combining travel time tomography (TTT) and inversion time migration (RTM) technology. This method can image the size and shape of voids in CFSTs with high resolution. Liu et al. [52] proposed an ultrasonic array imaging method based on full-matrix capture (FMC), which can semi-quantitatively characterize the voids of CFSTs. Liu et al. [52] used this method to detect the void in a CFST and verified the test results by core drilling method. The results show that the method has good detection accuracy and can adequately locate the void in a CFST. Although the ultrasonic method has been widely used in engineering to detect the void of CFST, the method still has the shortcomings of limited penetration and the influence of concrete aggregate on the detection results [53]. In addition, ultrasonic testing requires scanning the entire structure, which takes a long time, and, especially for large CFST arch bridge structures, the detection time will be longer.

The impact–echo method was first proposed by Sansalone and Carino of Cornell University in the United States [54]. This method uses the propagation and reflection of high-frequency sound waves generated by tapping the surface of the measured object in the concrete structure to detect defects. The waveform and spectrum of the impact elastic wave are analyzed to determine the location, size and boundary of the defect [55,56]. In recent years, due to the rapid development of machine learning, many scholars have used machine learning to optimize the impact–echo method [57,58]. Chen et al. [59] carried out the void detection test on a CFST based on the impact–echo method. The power spectral density (PSD) of the void area and the non-void area was extracted, and its features were used as the database of the support vector machine (SVM) model. The detection accuracy of the void detection model obtained by machine learning can reach 94.17%. The impact-echo method can well characterize the depth and shape of the void. However, the impact-echo detection is mainly affected by the impact error of the impact hammer and the installation error of the sensor. In actual use, it is difficult for the operator to accurately control the angle and amplitude of the impact. It is usually accompanied by a double hit in the impact process, resulting in a decrease in detection accuracy [60]. At the same time, the detection efficiency of the impact–echo method is very low, and it is required to detect the area to be measured point by point. For the CFST arch bridge, it is difficult to detect the whole arch rib.

The distributed optical fiber sensor has been widely used in civil engineering in recent years [61]. It uses the optical fiber itself as a sensor to continuously monitor the optical fiber along the length direction. The principle is to receive and analyze the scattered light by the optical time-domain reflectometer (OTDR) to obtain its attenuation waveform to determine the range, location and value of the void and crack [44,45]. Ding [44] obtained the semi-empirical formula of loss by a regression analysis of experimental data. At the same time, based on the force-light constitutive model, Ding [44] proposed a quantitative algorithm for the void–crack of a CFST and applied it in the Wuxia Yangtze River Bridge. Gong et al. [62] proposed a distributed optical fiber detection method with active heating function based on Brillouin reflection and clarified the relationship between the void depth and the equivalent heat absorption coefficient (EHAC). This method quantitatively detects the void by monitoring the surface temperature of a CFST. The optical fiber sensor has good accuracy and can accurately monitor the amount of void. However, the optical fiber material itself is low in strength and expensive. In practical engineering, it is necessary to embed the optical fiber sensor in the concrete structure, which greatly improves the requirements for construction technology and reduces the service life of the sensor.

The application of infrared thermal imaging technology in civil engineering has been developed for a long time. Because of its lack of contact and high efficiency, it has been widely studied in structural non-destructive testing. When there is a void in the CFST, the thermal conductivity of the air in the void area is quite different from that in the non-void area, so there is a certain temperature difference between the two areas. Because the steel tube has good thermal conductivity, the void can be detected by the temperature difference of the outer surface of the CFST. Wang et al. [63] used the characteristics of the high thermal efficiency of a rubber heating belt to wrap and heat CFST specimens. The results showed that the heating method could effectively detect small defects with a thickness of 5 mm. Guo and Yan [64] used eddy current thermal excitation method to explore the influencing factors of the internal hole detection of a CFST and established the multiple regression relationship between defect size, thickness of steel tube, heating time, heating power and heating rate. Jiang and Chen [65] used pulse heat source to heat the specimen, and the temperature difference between the surface of the specimen above the defect and other areas appeared via heat conduction. Due to the large pulse energy, the signal-to-noise ratio of the obtained heat map was improved. Because the detection results of the infrared thermal imaging method are finally presented as infrared thermal imaging images, many scholars have used image processing algorithms to improve the detection accuracy in recent years. Zhang et al. [66] used contrast limited adaptive histogram equalization (CLAHE) algorithm to solve the problem of gray loss and image patch in traditional algorithm, effectively

reducing the excessive distortion of local area contrast and regional noise interference and making the image of the defect area and the non-defect area clearer and more complete after processing. Zheng and Tan [67] combined the time domain fitting with the CLAHE algorithm to enhance the image and processed the edge image of the internal defects of the concrete in detail so that the recognition effect of the defects was improved. The infrared thermal imaging method has the advantages of non-contact detection, large-area detection and rapid detection. However, the infrared thermal imaging method also has certain shortcomings. The existing numerical simulation [65] has demonstrated that the void monitoring of CFSTs using the thermal imaging method is influenced by various factors, including the geometric dimensions of defects and the thickness of the steel tubes. Thicker steel tubes lead to a more uniform surface temperature distribution, making void monitoring challenging in large-scale CFSTs. Furthermore, the surrounding environment also influences the surface temperature field of CFSTs, which in turn affects the monitoring process. Moreover, this testing approach requires specialized heat equipment and involves a complex testing system [68].

Different detection methods have their own advantages and shortcomings in practical engineering applications. Therefore, the detection principles, advantages and shortcomings of the above methods are sorted out in Table 2.

Table 2. Advantages and shortcomings of various methods.

Methods	Detection Principles	Advantages	Shortcomings
Ultrasonic method	The difference in propagation velocity of ultrasonic wave in different media is used for detection.	The equipment is simple, and the detection cost is low.	Contact point-by-point measurement has slow detection speed. The penetration of ultrasonic wave is limited and easily affected by factors such as aggregate size.
Impact–echo method	The spectrum analysis of the P wave generated by hammering is performed to determine whether there is a void in the detection area.	The detection accuracy is high, and the depth and shape of the void can be well characterized.	Using contact point-by-point measurement, the detection speed is slow. It is difficult for operators to accurately control the angle and amplitude of the impact, resulting in errors.
Optical fiber sensor method	The scattered light is received and analyzed to obtain the attenuation waveform to determine the value, location and range of the void and crack.	The fiber optic sensor has good accuracy and can accurately monitor the degree of voids	The optical fiber sensor is expensive and needs to be embedded in concrete. The sensor is fragile, and the durability is poor.
Infrared thermography	The temperature field of the void area is different from the temperature field of the non-void area to distinguish the void.	Using non-contact remote detection, the detection range is large, and the detection speed is fast.	Only the surface void can be detected, and the detection accuracy is not high due to the limitation of weather and excitation mode.

2.3. Stress Detection

The bearing capacity of an arch bridge structure has always been a hot issue in engineering and academia. Both reinforced concrete structures and steel structures are important bearing components, and their stress state is an important index to measure the safety performance of an arch bridge [69]. At present, the detection methods of steel structure stress are mainly divided into the destructive detection method and the non-destructive detection method [70].

Destructive detection mainly refers to the stress release method. The principle is to partially destroy the area to be measured to release the stress in the area [71]. The strain of the region before and after the stress release is different due to the elastic deformation, so the stress magnitude and distribution of the region can be obtained by measuring the strain.

The hole-drilling method is a relatively mature stress detection method, which is widely used in engineering [72]. When using the drilling method to measure stress, it is necessary to paste the strain flowers at the position to be measured first. When the stress has been released, the strain gauge can measure the strain generated at the position, and the stress in

the area to be measured is obtained by using the correlation formula. Ju et al. [73] measured the residual stress distribution on the surface of 304 stainless steel via the drilling method, and the measurement results were consistent with the finite element simulation results. The stress was the smallest in the middle and gradually increased to both sides in both vertical and horizontal directions. Bobzin et al. [74] measured the residual stress distribution along the depth direction of the aluminum-based coating of the steel structure by the drilling method and found that the heat treatment had a relaxation effect on the residual stress level of the coating. Mohamed et al. [75] measured the residual stress of stainless steel coatings with different thicknesses by the drilling method. It was found that the residual stress of the coating at all thicknesses was tensile stress, and the bonding layer did not seem to affect the stress field. The advantage of drilling method is that the technology is mature, and the principle and operation are simple, but its measurement accuracy is easily affected by external test conditions, such as strain gauge sticking manners, drilling depth and so on, which will have a great impact on the accuracy of the measurement results [76].

The basic principle of the ring core method is to fully release the residual stress by machining an annular groove on the surface of the rotor. By pasting a strain gauge on the surface of the rotor, the electrical signal is converted into a strain value by the instrument, and finally, the stress size and direction are calculated [77,78]. In the experimental test research, Li and Ren [79] used the ring core method to detect the micro-indentation residual stress on the surface of steel structure specimens and combined it with ISSR technology to realize the distribution identification of residual stress. Hu et al. [80] used the ring core method combined with the three-dimensional digital image method to detect the residual stress on the surface of the steel plate, and the results were in good agreement with the theoretical model. Dang et al. [81] used the ring core method to evaluate the residual stress state of the double-layer film and obtained a feasible semi-destructive method.

The grooving method is an improvement based on the ring core method. The purpose is to facilitate cutting, and the release of stress is generated by cutting a linear or square groove on the material. The grooving method is easy to operate in practical engineering, causes less damage to the steel structure and is suitable for low-level stress measurement [82]. In the experimental test, Zhu et al. [83] studied the high temperature release law of residual stress on the surface of alloy materials by using the grooving method combined with an FIB-EB double-beam system. Shomali et al. [84] used the grooving method to test the shear performance of reinforced RC beams and carried out numerical analysis to verify the accuracy of the method. Yan et al. [85] carried out the grooving method for reinforced concrete specimens and analyzed the effects of different initial stresses, grooving methods and grooving depths on stress release efficiency. The detection principles, advantages and shortcomings of the above methods are sorted out in Table 3.

Table 3. Comparison of destructive detection methods.

Detect Methods	Advantages	Shortcomings	Detection Principles
Hole-drilling method	The technology is mature, and the principle and operation are simple.	The measurement accuracy is easily affected by many external factors.	Correlation between stress and strain
Ring core method	The accuracy and sensitivity of measurement are higher than those of the drilling method.	The operation is complex, and the processing process easily affects the material and stress.	
Grooving method	It is easy to operate and causes less damage to the steel structure.	The vibration of the cutting machine will disturb the strain test.	

Nondestructive testing has the advantages of not destroying structural integrity and being able to measure the same position multiple times to reduce measurement errors [86]. At present, the commonly used non-destructive testing methods for the stress state of key structures of arch bridges mainly include the resistance strain gauge method, X-ray diffraction method, magnetic measurement method and ultrasonic method.

The resistance strain gauge method is to paste the resistance strain gauge on the surface of the measured component. The sensitive gate of the strain gauge will change the resistance of the strain gauge due to the small deformation of the surface after the component is stressed [87,88]. According to the resistance strain effect, the strain at the strain gauge can be obtained, and then according to the elastic relationship between stress and strain, the purpose of obtaining the stress value of the component can be achieved. This method is common in test and measurement work. Kovačič et al. [89] verified the accurate characteristics of this method for bridge load test and measurement via signal processing examples measured by strain gauges, induction sensors and total stations. Turan et al. [90] used strain gauge to detect the residual stress at the groove on the surface of steel and effectively analyzed different types of stress. Ma et al. [91] proposed a displacement estimation technique based on a finite impulse response filter by using a resistance strain gauge and realized the accurate monitoring for the structural state of long-span bridges by integrating strain and acceleration measurements. The advantage of the resistance strain gauge method is that the measurement accuracy and sensitivity are high, and the stability in the measurement process is good. However, only the strain of a point on the surface of the component in a single direction can be measured, and the stress distribution cannot be reflected.

The basic principle of the X-ray diffraction method is that the lattice strain of the material caused by the stress is consistent with the macroscopic strain obtained by the elastic theory [92]. X-rays are incident on the metal surface under stress, and the lattice strain is calculated according to the Bragg diffraction equation, and the stress can be further calculated [93]. Monin et al. [94] measured the residual stress distribution of the welded joint by X-ray diffraction method and compared it with the residual stress state obtained by finite element analysis. Epp et al. [95] measured the radial residual stress intensity and distribution inside the steel hole extrusion strengthening parts using the X-ray method and analyzed the phase change characteristics of the crystal structure. Based on the inherent mean value of stress provided by X-ray diffraction, Morin et al. [96] inverted the linear system constructed by the average data set, developed a spatial deconvolution technique to reconstruct the local stress field and obtained the spatial distribution of stress. The X-ray diffraction method has high measurement accuracy and accurate measurement results, but it has high requirements for the surface finish of the component, and the detection equipment is expensive and complicated. In addition, the penetration depth of X-rays can only reach tens of microns, and the stress inside the structure cannot be measured. Crucially, the X-ray diffraction method may be harmful to human health, and specialized protective equipment and inspection techniques are required.

The basic principle of the weak magnetic detection method is to determine the magnitude of the stress by the coupling relationship between the stress of the magnetic material and the change in its internal magnetic properties [97]. According to the magnetic properties of ferromagnetic materials in arch bridge structures, the internal stress state is speculated by collecting and analyzing the variation characteristics of the surface magnetic field of ferromagnetic materials, only relying on the excitation of the geomagnetic field [98]. This method was first proposed by Russian scholar Dubov et al. [99]. In recent years, the research on the detection of steel bar stress state in bridge engineering has gradually increased. Huang et al. [100] and Chen et al. [101] carried out the axial tensile test of Q235 steel and explored the relationship between the magnetic signal and the steel fatigue load and the feasibility of magnetic flux leakage detection to predict structural damage. Tong et al. [102,103] measured the magnetic field data of HRB400 steel bar at different stress stages and obtained the coupling effect of elastic load and plastic deformation on magnetic memory signal. Zhang et al. [104] carried out the tensile–tensile fatigue test on a defective steel plate. It was found that the weak magnetic field strength can accurately detect the fatigue area and component life, and the results showed high detection sensitivity. At the same time, the results showed that there are many factors affecting the detection of weak magnetic field signals, such as the initial residual state of the material, the external magnetic field and

the ambient temperature [105–108]. Therefore, the quantitative evaluation of the self-stress state of ferromagnetic components needs to be further studied.

The detection principle of the ultrasonic method is based on the acoustic elasticity theory; i.e., the change in stress state in elastic components will cause the change in ultrasonic propagation velocity [109]. In the stress detection of a steel structure of an arch bridge, the application of the ultrasonic method is very extensive. The commonly used ultrasonic types include transverse waves, longitudinal waves, LCR waves, surface waves, etc. According to the different detection objects, the appropriate ultrasonic type and method can be selected for detection. Pilarski and Rose [110] effectively detected the surface defects of steel joints according to the characteristics of ultrasonic transverse waves. Chaki et al. [111] used the interaction of longitudinal waves and transverse waves to effectively detect the tightening degree of bolts under the internal stress of a steel structure, and the reliability reached 95%. Liu et al. [112] optimized the existing LCR wave detection method and developed a new surface coupling agent, which improved the accuracy of LCR waves for steel stress measurement. Eremeyev et al. [113] used surface wave detection technology to detect and analyze the flatness and stress state of a steel tube cylindrical surface. The detection principles, advantages and shortcomings of the above methods are sorted out in Table 4.

Table 4. Comparison of nondestructive detection methods.

Nondestructive Means	Advantages	Shortcomings	Detection Principles
Resistance strain gauge method	The measurement accuracy and sensitivity are high, and the stability of the measurement process is good.	The strain gauge must be closely attached to the surface of the component, which cannot reflect the stress distribution.	Resistance strain effects
X-ray diffraction method	The measurement precision is high, and the result is accurate.	The surface finish of the component is required to be high, and the internal stress cannot be measured.	Bragg diffraction equation
Weak magnetic detection method	Non-contact measurement can be realized, and the detection speed is fast.	It is susceptible to external influences, and the measurement accuracy is poor.	Magneto-mechanical coupled effect
Ultrasonic method	This method is fast, convenient and suitable for on-line detection.	The transducer and coupling agent are needed, and the detection accuracy and spatial resolution are limited by the size of the transducer.	Acoustoelastic effect

2.4. Corrosion Detection

The durability of reinforced concrete is a difficult problem faced by the whole world. Steel corrosion, chemical erosion, concrete carbonization, freeze–thaw damage, alkali aggregate reaction and so on will cause insufficient structural durability, but the main reason for accelerating concrete damage is steel corrosion [114,115]. The corrosion of steel bars reduces the cross-sectional area and the strength of steel bars and leads to cracks on the surface of concrete [116], which leads to the deterioration of the structural performance of arch bridges and reduces the structural bearing capacity of arch bridges. At present, there are three main non-destructive testing methods for steel corrosion, which are the analytical method, electrochemical method and physical method [117–119].

The analytical method is to detect the degree of concrete cracks, the thickness of the protective layer, the type of steel bar, the initial chloride ion content and the carbonization degree of the concrete structure [120]; collect a large amount of information; and analyze the information. Finally, the mathematical model of steel bar corrosion is established to achieve the purpose of predicting the degree of steel bar corrosion. The crack backstepping method after concrete cracking is the main method of analysis. Since the corrosion rate of steel bars in reinforced concrete exceeds a critical corrosion rate, it will lead to cracking

on the surface of concrete. Therefore, the degree of corrosion of internal steel bars is inversely deduced by the information of crack width after concrete corrosion expansion and cracking. Alonso et al. [121] carried out the corrosion test of reinforced concrete and analyzed the cracking law of the concrete protective layer under various water–cement ratios and thickness–diameter ratios. Liang and Wang [122] analyzed the thick-walled cylinder corrosion model and verified the model's prediction of the cracking time of the concrete cover using the measured data.

The process of concrete cover cracking caused by steel bar corrosion is quite complicated. The research on the process of concrete corrosion damage at home and abroad is mainly focused on the pre-cracking. Based on experimental research and theoretical analysis, the calculation formula of the corrosion rate of a steel bar section during cracking is given directly or indirectly. The development process of rust expansion and its influencing factors are simulated and analyzed by the nonlinear finite element method, but the relationship between the width of a rust expansion crack and the corrosion rate of a steel bar is rarely given. Using the rapid corrosion test, the calculation formula of the corrosion rate of the steel bar section based on the width of the corrosion expansion crack is given directly or indirectly. Throughout some of the existing research results, the Table 5 lists several theoretical calculation models for the loss rate of steel corrosion W loss and crack width w after concrete surface cracking.

Table 5. Theoretical calculation model of steel corrosion loss rate and crack width after concrete surface cracking.

Theoretical Model	Computational Expressions	Main Technical Indexes
Di model [123]	$W_{loss\ rate} = \begin{cases} 507 \cdot e^{0.007c} \cdot {f_{cu}}^{-0.09} \cdot d^{-1.76} \\ (w \le 0.2 \text{ mm}) \\ 332 \cdot e^{0.008c} \cdot {f_{cu}}^{-0.567} \cdot d^{1.108} \\ (0.2 \le w \le 0.4 \text{ mm}) \end{cases}$	c: concrete cover depth f_{cu}: concrete strength d: bar diameter w: crack width
Hui model [124]	Class I round rebar at the corner: $W_{loss\ rate} = (32.43 + 0.303 f_{cu} + 0.65c + 27.45w)/d$ Threaded Class II rebar at the corner: $W_{loss\ rate} = (34.486w + 0.789 f_{cu} - 1.763)/d$ Grade I round steel bars located at the stirrup position: $W_{loss\ rate} = (276w + 1.07 f_{cu} + 59.45)/d$	c: concrete cover depth f_{cu}: concrete strength d: bar diameter w: crack width
Niu model [125]	$W_{loss} = 1.173 \cdot P_{RH} \cdot D_0 \cdot (t - t_{cr})$	P_{RH}: correction coefficient of environmental humidity D_0: oxygen diffusion coefficient
Wang model [126]	$W_{loss\ rate} = 4[(0.2345w + 0.0175)/d - (0.2345w + 0.0175)^2/d^2]$	d: bar diameter w: crack width
"Durability evaluation standard of concrete structure" GB/T51355-2019 [127]	Corner round steel bar: $W_{loss\ rate} = \begin{cases} 0.07w + 0.012c/d + 0.00084 f_{cu} + 0.08 \\ (w \ge 0.33 \text{ mm}) \\ 0.35w + 0.012c/d + 0.00084 f_{cu} - 0.013 \\ (w < 0.33 \text{ mm}) \end{cases}$ Angular deformed steel bar: $W_{loss\ rate} = \begin{cases} 0.086w + 0.008c/d + 0.00055 f_{cu} + 0.015 \\ (w \ge 0.10 \text{ mm}) \\ 0.35w + 0.008c/d + 0.00055 f_{cu} - 0.013 \\ (w < 0.10 \text{ mm}) \end{cases}$	c: concrete cover depth f_{cu}: concrete strength d: bar diameter w: crack width
Mao model [128]	$W_{loss\ rate} = 2.9598w + 1.5647$	w: crack width
Andrade model [129]	$W_{loss\ rate} = 4[(0.222w - 0.011)/d - (0.222w + 0.011)^2/d^2]$	d: bar diameter w: crack width

The corrosion of steel bars in concrete is an electrochemical process, so the electrochemical detection method can be used as a powerful means to reflect the degree of corrosion of steel bars [130]. The half-cell potential (HCP) method is the most widely used detection method in the electrochemical method. When the steel bar is corroded in the concrete, the primary battery is formed; that is, the anode area and the cathode area are formed on the surface of the steel bar. Between these regions, a micro-current will be generated inside the concrete, and the electrical activity of the steel bar and the concrete can be considered as a half-weak battery pack, where the steel bar acts as an electrode, and the concrete acts as an electrolyte [131]. The measurement method is to connect the steel bar to one end of the potentiometer, while the other end is connected with a reference electrode. The reference electrode moves on the surface of the concrete, and the relative potential difference between the steel bar electrode and the reference electrode in different regions is measured. As shown in Figure 8, the equipotential line on the surface of the concrete is drawn, and the equipotential zone is determined. The most negative part is the corrosion zone. The evaluation criteria of steel corrosion are as follows: when the potential is larger than −200 mV, the probability of no corrosion is greater than 90%; when the potential is −200 mV~−350 mV, the degree of corrosion is uncertain; when the potential is less than −350 mV, the probability of corrosion is larger than 90%. In previous research, Amiri et al. [132] used the HCP method to monitor the bridge deck corrosion of reinforced concrete bridges, and the method showed good accuracy and effectiveness. Adriman et al. [133] diagnosed the area and size of steel corrosion in reinforced concrete by combining the field data and simulation calculation of semi-unit potential measurement, and the accuracy rate reached 95.65%. Almashakbeh et al. [134] used the HCP method to investigate the effect of corrosion grade on the flexural capacity of reinforced concrete members and found a positive correlation between the measured value of semi-element potential and the flexural capacity of RC beams. And the flow chart of steel corrosion detection by half-cell potential method is shown in Figure 9.

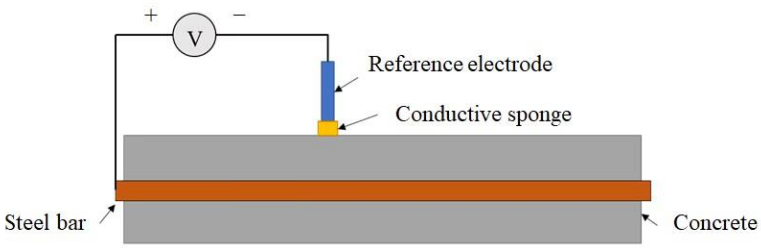

Figure 8. Half-cell potential method to detect steel corrosion schematic diagram.

Physical method tests are related to physical characterizations, including changes in electromagnetic, thermal, acoustic, and electrical resistance. And the changes are caused by steel corrosion [135]. The magnetic memory nondestructive testing method belongs to the magnetic field measurement method in the physical method, which is the research hotspot at the present stage. Under the combined action of a working load and the Earth's magnetic field, the ferromagnetic components of an arch bridge structure will undergo directional and irreversible reorientation of the magnetic domain structure with magnetostrictive properties in the corrosion concentration area and stress concentration area, resulting in the formation of a leakage magnetic field on the surface of the material [97]. By detecting the distribution of the leakage magnetic field on the surface of the ferromagnetic component, it can not only accurately judge the macroscopic defects that have been formed in the component but also detect the microscopic defects by other non-destructive testing methods such as ultrasound and eddy current. It can indicate the stress concentration position of the hidden defects and has the ability of early rapid warning [136]. The corrosion of steel bars in reinforced concrete is a prominent problem in the disease of arch bridges. Scholars have conducted a great amount of research on solving the problem of determining the corrosion area and corrosion degree of steel bars. Zhou et al. [137,138] first carried out the magnetic memory

signal detection test of steel corrosion in the reinforced concrete of a bridge structure. It was found that the tangential magnetic induction intensity in the steel corrosion area had a large magnetic anomaly, and the magnetic flux leakage intensity curves of different lift-off heights had intersection points in the corrosion area, which provided a strong magnetic memory criterion for the detection of steel corrosion width. Xia et al. [139,140] optimized the magnetic dipole model, explored the change characteristics of the magnetic memory signal under the conditions of corrosion and wire breaking in an arch bridge suspender structure, and established the relationship between corrosion degree and magnetic memory signal. Su et al. [141,142] explored the mechanical properties of steel bars and steel plates under different degrees of corrosion and used magnetic memory testing to effectively analyze the influence of the corrosion of steel specimens on service life. The magnetic field distribution in the corrosion area of steel plate can be found in Figure 10.

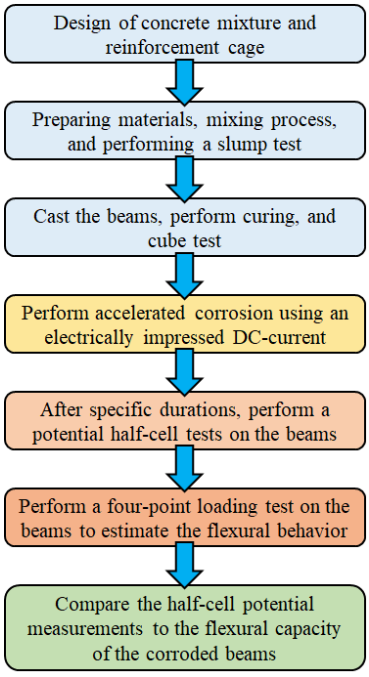

Figure 9. Flow chart of steel corrosion detection by half-cell potential method [134].

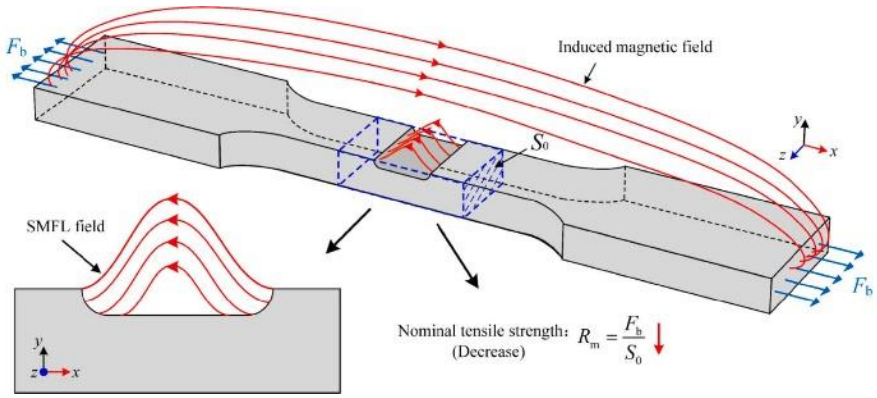

Figure 10. Magnetic field distribution in the corrosion area of steel plate [142].

3. Damage Identification for the Overall Performance of Arch Bridge

In addition to physical means (such as the ultrasonic method, magnetic memory method, etc.), the health monitoring system has also been widely used in the damage identification of arch bridges. Differently from the damage diagnosis method of arch bridges based on local detection data (such as acoustic wave, magnetic signal, etc.), the overall

damage identification method is mainly based on the structural vibration response obtained from the monitoring system [143,144]. The characteristic indexes of structural damage are defined by means of modal analysis or mathematical statistics. The damage occurrence, damage location or quantitative damage degree of the structure can be identified via the change in damage index. According to different development histories and construction materials, arch bridges can be divided into the following four types: masonry arch bridge, steel arch bridge, RC arch bridge and CFST arch bridge. In order to show the differences between damage identification methods caused by different structural characteristics comprehensively, the damage identification methods of a masonry arch bridge, a steel arch bridge and an RC arch bridge have been reviewed in the existing literature [145]. On this basis, this paper analyzes the relevant literature on the damage identification of arch bridges in the past five years, and the introduction of the damage identification method of a CFST arch bridge is added. The characteristics of damage identification methods for different types of arch bridges are summarized to show the latest progress on arch bridge damage identification methods more comprehensively and systematically.

3.1. Masonry Arch Bridge Damage Identification Method

The masonry arch bridge has a long history because the materials used are mostly stone. The early structural forms are mainly circular arc and filled spandrel arch bridges, and the span is short. Stone arch bridges, including Zhaozhou Bridge, have become precious cultural heritage sites. However, due to the long-term erosion of the natural environment, a large number of structural diseases have occurred in masonry arch bridges, and the structural performance degradation is serious. In order to better maintain and retain such cultural heritage, scholars have tried various methods, and they carry out research on the damage identification of masonry arch bridges. Some scholars use the structural response data obtained by traditional sensing methods to realize damage identification by means of modal analysis or finite element model correction [146]. For example, Serra et al. [147] simulated the foundation displacement of a 1: 2 scale masonry arch bridge model in the laboratory and obtained the acceleration along the structure generated by hitting the bridge wall with a hammer. The coda wave interferometry was used to detect the change in the elastic properties of the medium. Furthermore, the evolution of the structural damage mechanism was analyzed. Emre [148] focused on the scale model of a single-span historical masonry arch bridge in the laboratory and used the enhanced frequency domain decomposition (EFDD) technology to identify the operating mode of the bridge. The ANSYS finite element of the structure was modified via response surface methodology to realize the approximate identification of the damage location. Civera et al. [149] proposed a fast relaxation vector fitting (FRVF) method for the fast, effective and reliable identification of structural systems based on vibration. The results show that this method can match other mature SI technologies well, such as the Eigensystem Realization Algorithm (ERA), and can be used for damage assessment. On this basis, they combined machine learning and operational modal analysis to propose a novel automatic OMA multi-stage clustering algorithm and applied it to the damage detection and damage degree assessment of masonry arch bridges [150]. Conde et al. [151] obtained the most probable distribution of the finite element model parameters by using a Bayesian method and the Markov chain Monte Carlo (MCMC) method based on the comparison between the finite element calculation results and the actual measured geometric data so as to reproduce the existing damage mode with the highest accuracy using the numerical model. The results showed that the proposed method could reasonably infer the original geometric structure of the bridge and the possible damage loading scene so as to obtain the crack mode, which was almost the same as the current damage state. Borlenghi et al. [152] analyzed the damage and operation mode of a long-standing masonry arch bridge, Olla bridge, via visual inspection and a field test, and modified the finite element model of the structure based on the measured data. Alexakis et al. [153] used acoustic emission sensors to study the deterioration of masonry structures under gradually increasing cyclic loading. The results showed that the acoustic

emission results had a significant correlation trend with different damage stages. Based on this, a real-time warning system for early structural damage can be developed.

Other scholars use advanced measurement methods to obtain the key geometric parameters of masonry arch bridges in service and realize structure damage identification by modifying the finite element model. For example, Pepi et al. [154] combined advanced measurement procedures, such as close-range photogrammetry based on drones and environmental vibration testing, to propose a finite element model correction method for severely damaged historical masonry structures and to guide the structure damage assessment. Batar et al. [155] used terrestrial laser scanning (TLS) technology to determine the geometric shape of the bridge with high precision. Based on the obtained point cloud data, a three-dimensional CAD-based structural solid model was established. The CDP material model was used to describe the inelastic behavior of the homogeneous structure, and then the structural behavior was analyzed with high precision and reliability. Deng et al. [156] proposed an automatic identification method for the arch axis of a stone arch bridge based on 3D laser scanning and applied it to Lugou Bridge with a history of 800 years. The results show that the relative deformation of the upstream and downstream arch rings of the bridge and the relative deviation of the arch rise and span of the belly arches at symmetrical positions are significant.

In addition, relevant scholars have paid attention to the identification and evaluation of seismic damage of arch bridges. For example, Jara et al. [157] established a numerical model based on the disease data of bridges. By revealing the failure mechanism of different types of structural members, the effects of epicentral distance and seismic fault on the seismic vulnerability of bridges were evaluated. By performing a series of environmental vibration tests, the dynamic characteristics of five existing historical bridges were determined, which could be used to construct the vulnerability curve and determine the numerical model of bridge seismic vulnerability. In order to investigate the seismic performance of damaged masonry arch bridges, Kaya et al. [158] simulated different damage states using a shaking table test. Then, based on the environmental vibration test, the structural modal parameters under undamaged and damaged conditions were obtained. The experimental results were in good agreement with the numerical simulation results, which provided a reference for the damage assessment of masonry arch bridges after earthquakes. Considering the uncertainty of material properties and seismic input, Gönen et al. [159,160] used a 3D finite element model for probabilistic nonlinear analysis, combined with a Monte Carlo simulation and first-order reliability method (FORM), to propose a probabilistic evaluation method for the seismic performance of masonry arch bridges.

3.2. Damage Identification Method of Steel Arch Bridge

The steel arch bridge is sensitive to the stiffness change caused by damage, which will lead to changes in structural modal characteristics. Therefore, most of the damage identification methods of steel arch bridges are based on structural modal characteristics. Due to the certain impact of environmental factors on the modal characteristics of structures, the existing literature has studied variations in the modal characteristics of steel arch bridges under environmental influences, aiming to further improve the accuracy of damage identification by eliminating the impact of environmental factors. For example, Mu et al. [161] used Bayesian network to model the relationship between the long-term monitoring data (temperature, humidity, wind speed and traffic volume) and the modal frequency of Xinguang Bridge (a 782 m steel arch bridge). The results showed that the selected network structure adequately captured the relationship between modal frequency and multiple environmental factors. Anastasopoulos et al. [162,163] used fiber Bragg grating strain sensors to continuously monitor a steel arch bridge for two years, automatically identifying the fundamental frequency and vibration modes of the structure from the measured strain time history. The results showed that the temperature had a great influence on the fundamental frequency but only had a slight effect on some high-order modes. In addition, the finite element simulation confirmed that the local damage had a significant

effect on the modal characteristics of the structure. Considering the bearing characteristics and spatial temperature distribution, Zhu et al. [164] discussed the relationship between the temperature change and temperature response of a long-span steel truss arch bridge with spherical bearing by using elastic beam theory and verified it using field monitoring data. The results showed that this relationship was determined by the structural parameters, especially the section characteristics and bearing characteristics of the bridge. Based on this, the criterion of bridge state identification could be established. Combined with correlation analysis, numerical simulation and neural network technology, Teng et al. [165] studied the mechanism of the influence of temperature on the structural frequency. The results showed that the modal frequency of the arch was mainly affected by the change in elastic modulus. Sunca et al. [166] used EFDD and the stochastic subspace identification method to identify the modal parameters of an Eynel steel arch bridge in the frequency domain and time domain, respectively. The results showed that the change in natural frequency was very limited, and there was no change between the vibration modes, which was in line with the actual situation of the bridge.

Some scholars have identified the occurrence of structural damage based on changes in the natural frequency, vibration modes or modal damping of steel arch bridges. For example, Chiaia et al. [167] used modal analysis technology and a data-driven stochastic subspace identification algorithm to extract the dynamic characteristics of the structure, including natural frequency, damping ratio and vibration modes, and then identify the damage of the structure. Dammika et al. [168] believed that structural damage would lead to changes in structural stiffness and damping characteristics, thereby changing the natural frequency, vibration mode and modal damping ratio of the structure. The energy-based damping model was introduced to estimate the damping parameters such as the equivalent loss factor of the structural members of the steel arch bridge, and the modal damping ratio of the bridge was analyzed by using the damping parameters. The results show that the method could identify the damping source of the steel bridge and its contribution to the modal damping ratio. Tran and Ozer [169] identified modal parameters based on the information matrix system implementation method. Then, the damage of the structure was identified from the stable modal poles collected from the stability diagram via the anomaly detection algorithm based on Gaussian distribution. Whelan et al. [170] monitored the environmental vibration of a tied arch bridge using a wireless sensor network and then estimated its modal parameters. In the parallel computing cluster, the integer-constrained genetic algorithm was used to optimize the objective function globally to update the cross-scale finite element model so as to evaluate the damage state of the structure.

Furthermore, some scholars define the damage sensitivity index to characterize the damage location or degree of the structure according to the structural modal parameters so as to realize the damage location and damage degree quantification of the steel arch bridge. For example, Jayasundara et al. [171] used the dual-criteria method based on modal flexibility and modal flexibility change to identify and locate the damage of steel arch bridges. The results showed that under certain damage conditions, the damage of arch ribs and longitudinal columns can be detected and located accurately via only a small number of early vibration modes. On this basis, Jayasundara et al. [172,173] proposed a vibration-based damage location and quantification method for arch bridge ribs. Based on the change of damage mode of frequency response functions (FRFs), the location and severity of structural damage are predicted by artificial neural networks (ANNs). Based on the nonlinear and non-stationary dynamic response of bridges, Delgadillo et al. [174] used Hilbert–Huang transform and instantaneous phase difference to construct damage sensitive features. Furthermore, the damage under traffic transient vibration was detected, located and quantified. The artificial damage of a real steel arch bridge was identified. The results showed that the proposed method had good robustness and sensitivity. Based on the seismic acceleration response signal, Kordestani et al. [175] calculated the energy level according to the Arias strength and normalized it to locate the damaged suspender.

Using the three-dimensional numerical simulation of the tied arch bridge under 16 different ground motions, the effectiveness of the method was verified.

3.3. Damage Identification Method of RC Arch Bridge

Similarly to the damage identification method of a steel arch bridge, the damage identification method of an RC arch bridge is mostly based on the modal parameters of the structure. For example, Magalhães and Cunha [176] proposed three effective output-only modal identification algorithms. By processing the test data of a concrete arch bridge with a span of 280 m, the steps of these identification procedures were clarified. At the same time, the operational modal analysis under the background of structural health monitoring was introduced. Furthermore, based on the environmental excitation response of an RC arch bridge, Magalhães et al. [177] used the automatic operation modal analysis algorithm to identify the modal parameters of the bridge online. By reducing the influence of environmental and operational factors on the natural frequency of the bridge. The evolution law of the modal characteristics of the bridge over time in the past two years is obtained, and the damage identification is carried out by using the control chart. The results showed that the proposed method could detect the real damage scene related to the frequency shift of about 0.2%. Ren et al. [178,179] proposed a new damage feature of a vibration system by using the system matrix based on covariance-driven stochastic subspace identification. In order to reduce the influence of modeling error, noise and environmental changes on the response of the measurement structure. The statistical pattern recognition paradigm was added to this method. By defining the damage index based on statistics, the Mahalanobis and Euclidean distance judgment functions of the damage feature vector were used. And the method was verified by the reinforced concrete beam tested in the laboratory and the full-scale arch bridge tested in the field. Based on multivariate statistical techniques, Comanducci et al. [180] processed the monitoring data of arch bridges and defined damage-sensitive features under changing environments and operating conditions. It was applied to the time history of the modal frequency of the bridge, and the control chart was used to evaluate its ability to reveal structural damage of varying severity. Ferrari et al. [181] identified the structural modal characteristics based on the collected experimental vibration data. Combined with Latin hypercube sampling, a self-fulfilling global optimization method for model updating was proposed. It had been successfully applied to a century-old reinforced concrete parabolic arch bridge with historical significance. Based on the Fourier amplitude spectrum (FAS) of acceleration response, Duan et al. [182] used a CNN to identify the damage of suspenders of tied arch bridges. The results showed that the CNN had good robustness under various observation noise levels and wind speeds.

In addition, scholars have also explored some novel damage identification methods for RC arch bridges, including data-driven methods and methods based on radar interferometry. For example, Zhou et al. [183] proposed a damage identification method for RC arch bridges based on monitoring data. The acceleration data were preprocessed by a Kalman filter and an autoregressive moving average (ARMA) model. The damage index was constructed, and the identification accuracy was further improved by the generalized autoregressive conditional heteroscedasticity (GARCH) model. Qin et al. [184] used a modern differential interferometric synthetic aperture radar (DInSAR) to improve the reliability of PT identification, thermal expansion separation and the structural risk assessment of arch bridges. Taking Rainbow Bridge and Lupu Bridge as examples, the effectiveness of the method was verified. And the experimental results were verified by horizontal benchmark verification, cross-sensor comparison and structural reliability evaluation.

3.4. Damage Identification Method of CFST Arch Bridge

The damage identification method of a CFST arch is different from that of other types of arch bridges. Due to the particularity of CFST arch bridge structure and material, its damage identification is mainly based on static means. For example, Wang et al. [185]

established the relationship between the static deflection change of the suspender and the cable force. Based on the static deflection difference, the damage identification index of the suspender was proposed. The numerical simulation and experimental results show that the method can accurately locate the damage location and give the relative damage degree. Li et al. [186] combined monitoring data and detection data to modify the finite element model from the component and global, respectively. Thus, several common defects of a CFST arch bridge were investigated and updated. Fu and Jiang [187] proposed a new intelligent damage detection data fusion system by combining a probabilistic neural network (PNN), data fusion technology and correlation fractal dimension (CFD). Single and multiple damage modes were identified by the numerical simulation of a two-span CFST arch bridge. The results showed that the hybrid data fusion system had good damage identification performance, anti-noise ability and robustness. Gui et al. [188] analyzed the ultimate bearing capacity modeling, limit threshold setting and limit state prediction of concrete-filled steel tubular members. A system maintenance decision model was proposed, which combined the relative monitoring state, the relative final state of numerical analysis and the relative residual life of degraded components. The results showed that these technologies had great potential for the life cycle performance evaluation of the existing concrete bridge structure health monitoring system.

In addition, scholars have also made some explorations on the damage identification methods of CFST arch bridges using modal characteristics. For example, Yan and Ren [189] took the idea that the power spectral density transmittance (PSDT) was independent of the external excitation and the transmitted output of the system poles. It was proposed to extract the working modal parameters of the structure based on PSDT, which was verified and analyzed by a half-arch bridge of CFST. The recognition results were compared with those of the peak picking method, random subspace identification and finite element analysis. The results showed that the working modal parameters identified by this method were in good agreement with other methods and had the potential to be applied to structural damage identification. Xiong et al. [190] used the global navigation satellite real-time kinematics system to monitor the vibration response of long-span CFST arch bridges under environmental excitation. The structural modal parameters were calculated by fast Fourier transform and a random decrement technique.

Based on the above study, the damage indexes of damage identification for the overall performance are summarized in Table 6.

Table 6. Damage indexes of damage identification for the overall performance.

Damage Index	Computational Expressions	Main Parameter
Modal flexibility damage index [171]	$MFDI_{ij} = \frac{\left[\sum_{i=1}^{m} \frac{1}{\omega_i^2} \phi_i \phi_i^T\right]_D - \left[\sum_{i=1}^{m} \frac{1}{\omega_i^2} \phi_i \phi_i^T\right]_H}{\left[\sum_{i=1}^{m} \frac{1}{\omega_i^2} \phi_i \phi_i^T\right]_H}$	m: the mode number ω_i: the natural frequency of the structure at mode i ϕ_i: ith mode shape vector D: the damage conditions H: the healthy conditions
Modal strain energy damage index [172]	$\beta_{ij} = \frac{k_j}{k_j^*} = \frac{\left[(\phi''^*_i)^2 + \sum(\phi''^*_i)^2\right]\left[\sum(\phi''_i)^2\right]}{\left[(\phi''_i)^2 + \sum(\phi''_i)^2\right]\left[\sum(\phi''^*_i)^2\right]}$	β_{ij}: Modal strain energy damage index for jth member at ith mode k_j: the bending stiffness of the beam $\phi_i(x)$: the mode shape of ith modal vector
Normalized arias intensity [175]	$I_A = \frac{\pi}{2g}\int_0^T a^2(t)\mathrm{d}t$ $\beta_i = \frac{I_{A-IN_i}}{\overline{I_{A-IN}}}$ $NI_{A_i} = \frac{I_{A-DM_i}}{\overline{I_{A-DM}}} \times \frac{100}{\beta_i} = \frac{I_{A-DM_i}}{\overline{I_{A-DM}}} \times \frac{\overline{I_{A-IN}}}{I_{A-IN_i}} \times 100$	I_A: arias intensity T: duration of acceleration a: acceleration data β: normalizing factor i: the node counter NI_A: normalized arias intensity I_{A-IN}: arias intensity for intact condition I_{A-DM}: arias intensity for damaged condition

Table 6. *Cont.*

Damage Index	Computational Expressions	Main Parameter
Statistics-based damage index [178]	$NI_{i,\gamma}^{E} = \frac{\overline{D}_{i,T}^{E}}{\overline{D}_{i,J}^{E}}$ or $NI_{i,\gamma}^{M} = \frac{\overline{D}_{i,T}^{M}}{\overline{D}_{i,J}^{M}}$	$\overline{D}_{i,T}^{E}$: The mean value of Euclidean of the state to be evaluated $\overline{D}_{i,J}^{E}$: The mean value of Euclidean of baseline state
Deflection-based identification index [185]	$DI = \Delta w(i+2) - 2\Delta w(i+1) + 2\Delta w(i-1) - \Delta w(i-2)$	$\Delta w(i+2)$, $\Delta w(i+1)$, $\Delta w(i-1)$ and $\Delta w(i-2)$ are the static deflection changes at nodes i + 2, i + 1, i − 1 and i − 2 before and after hanger damage, respectively
Transmissibility-based damage index [191]	$DI(T_{ud}, T_d) = \frac{\|\|\{T_{ud}\}\| - \|\{T_d\}\|\|}{\|\|\{T_{ud}\}\| + \|\{T_d\}\|\|}$	T_{ud}: transmissibility matrices from the slab response to the girder response in undamaged states T_d: transmissibility matrices from the slab response to the girder response in damaged states

4. Conclusions

This paper reviews the research progress of damage monitoring and identification methods for arch bridges, including damage monitoring for local diseases of arch bridges and damage identification for the overall performance of arch bridges. The main conclusions are as follows:

(1) In the monitoring of local disease damage, the principles of various methods and their advantages and shortcomings are summarized. According to the different damage parts, the different damage types (cracks or aging, corrosion, fractures or cracks, and anchorage efficiency decrease) and the commonly used methods (the machine vision method, magnetic flux leakage detection method, acoustic emission method, magneto strictive guided wave detection method, and piezoelectric sensor method) are summarized from three aspects of an HDPE sheath, the internal steel wire of the cable body and the anchorage system. At present, there are four commonly used methods for void monitoring: the ultrasonic method, impact–echo method, optical fiber sensor method and infrared thermal imaging method. The stress detection of the main bearing components of the arch bridge is divided into two categories: destructive detection and non-destructive testing. The destructive detection mainly includes the drilling method, ring core method and segmentation grooving method. The non-destructive testing mainly includes the resistance strain gauge method, X-ray diffraction method, weak magnetic detection method and ultrasonic method. There are three main non-destructive testing methods for steel corrosion detection, i.e., the analysis method, electrochemical method and physical method (electromagnetic method, heat conduction method, acoustic emission method and resistance method). In the Introduction and summary, it is found that non-destructive testing is the research focus of the local disease damage monitoring of arch bridges. Among them, the physical method can include most of the detection methods, and the other methods can be divided into machine vision methods and sensor methods.

(2) In the damage identification of the overall performance, the modal-based damage identification is still the main research direction. In addition to the static damage identification of the CFST arch bridge, the other three bridge types are mainly based on modal-based damage identification. In the masonry arch bridge, the traditional sensing method and the advanced measurement method are taken into account. In addition to the modal analysis, the finite element model correction method is also introduced to identify the damage. At the same time, the identification and evaluation of seismic damage have also attracted the attention of scholars. Most of the research on steel arch bridges is based on modal characteristics. In order to achieve high-accuracy identification, the variation law of the modal characteristics of steel arch bridges under environmental influence is studied to eliminate the influence of environmental factors. The damage sensitivity index is also proposed to realize the damage location and damage degree quantification of steel arch bridges. In addition to the modal research of RC arch bridges, scholars have also explored some novel methods, including data-driven methods and methods based on radar

interferometry. Although CFST arch bridges are mainly based on static means, scholars have also made some explorations on the modal-based damage identification method.

(3) It can be found that the applicability and effectiveness of different available techniques depend on the damage type, structural configuration and available data. However, a universal method that can identify all damage types of different structures remains to be developed. In addition, although some achievements have been made in damage monitoring and identification, it is still necessary to develop more accurate and reliable damage identification methods to realize the effective combination of local disease damage monitoring and overall performance damage identification. In particular, the research on the damage location method of the overall performance is imminent. Once the two-step strategy of "overall structural damage location" and "local disease damage monitoring" is realized, the efficiency of damage identification will be greatly improved, and the structure can also be accurately and timely repaired and maintained, thereby prolonging the service life of the structure.

Author Contributions: Conceptualization, J.Y. and J.X.; methodology, J.Y. and L.H.; investigation, K.T., Q.T. and H.L.; writing—original draft preparation, J.Y. and L.H.; writing—review and editing, J.Y. and J.X.; visualization, L.H., K.T. and H.C.; supervision, J.X.; funding acquisition, J.X. All authors have read and agreed to the published version of the manuscript.

Funding: The supports by National Natural Science Foundation of China (Grant No. 52278292), Chongqing Outstanding Youth Science Foundation (Grant No. CSTB2023NSCQ-JQX0029), Chongqing Science and Technology Project (CSTB2022TIAD-KPX0205), Chongqing Transportation Science and Technology Project (Grant No. 2022-01), Science and Technology Project of Guizhou Department of Transportation (Grant No. 2023-122-001), China Postdoctoral Science Foundation (Grant No. 2023M730431), and Special Funding of Chongqing Postdoctoral Research Project (Grant No. 2022CQBSHTB2053) are greatly acknowledged.

Data Availability Statement: Some or all data, models or code that support the findings of this study are available from the corresponding author upon reasonable request.

Conflicts of Interest: The authors declare no conflict of interest.

References

1. Zhang, H.; Li, H.; Zhou, J.; Tong, K.; Xia, R. A multi-dimensional evaluation of wire breakage in bridge cable based on self-magnetic flux leakage signals. *J. Magn. Magn. Mater.* **2023**, *566*, 170321. [CrossRef]
2. Xin, J.; Zhou, J.; Zhou, F.; Yang, S.; Zhou, Y. Bearing Capacity Model of Corroded RC Eccentric Compression Columns Based on Hermite Interpolation and Fourier Fitting. *Appl. Sci.* **2018**, *9*, 24. [CrossRef]
3. Chen, Z.; Xu, Y.; Hua, J.; Wang, X.; Huang, L.; Zhou, X. Mechanical Properties and Shrinkage Behavior of Concrete-Containing Graphene-Oxide Nanosheets. *Materials* **2020**, *13*, 590. [CrossRef] [PubMed]
4. Yang, J.; Chen, R.; Zhang, Z.; Zou, Y.; Zhou, J.; Xia, J. Experimental study on the ultimate bearing capacity of damaged rc arches strengthened with ultra-high performance concrete. *Eng. Struct.* **2023**, *279*, 115611. [CrossRef]
5. Hou, R.; Xia, Y. Review on the new development of vibration-based damage identification for civil engineering structures: 2010–2019. *J. Sound Vib.* **2021**, *491*, 115741. [CrossRef]
6. Wang, C.; Ansari, F.; Wu, B.; Li, S.; Morgese, M.; Zhou, J. LSTM approach for condition assessment of suspension bridges based on time-series deflection and temperature data. *Adv. Struct. Eng.* **2022**, *25*, 3450–3463. [CrossRef]
7. Tang, Q.; Xin, J.; Jiang, Y.; Zhou, J.; Li, S.; Fu, L. Fast identification of random loads using the transmissibility of power spectral density and improved adaptive multiplicative regularization. *J. Sound Vib.* **2022**, *534*, 117033. [CrossRef]
8. Zeng, Y.; He, H.; Qu, Y.; Sun, X.; Tan, H.; Zhou, J. Numerical Simulation of Fatigue Cracking of Diaphragm Notch in Orthotropic Steel Deck Model. *Materials* **2023**, *16*, 467. [CrossRef]
9. Xin, J.; Zhou, C.; Jiang, Y.; Tang, Q.; Yang, X.; Zhou, J. A Signal Recovery Method for Bridge Monitoring System Using TVFEMD and Encoder-Decoder Aided LSTM. *Measurement* **2023**, *214*, 112797. [CrossRef]
10. Xin, J.; Jiang, Y.; Zhou, J.; Peng, L.; Liu, S.; Tang, Q. Bridge Deformation prediction based on SHM data using improved VMD and conditional KDE. *Eng. Struct.* **2022**, *261*, 114285. [CrossRef]
11. Zeng, Y.; Qiu, Z.; Yang, C.; Haozheng, S.; Xiang, Z.; Zhou, J. Fatigue Experimental Study on Full-Scale Large Sectional Model of Orthotropic Steel Deck of Urban Rail Bridge. *Adv. Mech. Eng.* **2023**, *15*, 168781322311552. [CrossRef]
12. Li, S.; Xin, J.; Jiang, Y.; Wang, C.; Zhou, J.; Yang, X. Temperature-induced deflection separation based on bridge deflection data using the TVFEMD-PE-KLD method. *J. Civ. Struct. Health* **2023**, *13*, 781–797. [CrossRef]
13. Zheng, J.; Wang, J. Concrete-filled steel tube arch bridges in china. *Engineering* **2018**, *4*, 143–155. [CrossRef]

14. Zhang, L.; Qiu, G.; Chen, Z. Structural health monitoring methods of cables in cable-stayed bridge: A review. *Measurement* **2021**, *168*, 108343. [CrossRef]
15. Jafari, M.; Hou, F.; Abdelkefi, A. Wind-induced vibration of structural cables. *Nonlinear Dyn.* **2020**, *100*, 351–421. [CrossRef]
16. Abdullah, A.B.M.; Rice, J.A.; Hamilton, H.R. Wire breakage detection using relative strain variation in unbonded posttensioning anchors. *J. Bridge Eng.* **2015**, *20*, 04014056. [CrossRef]
17. Rizzo, P.; Enshaeian, A. Challenges in bridge health monitoring: A review. *Sensors* **2021**, *21*, 4336. [CrossRef]
18. Zhu, Z.; Wang, D.; Liu, C.; Wang, B. Research on wire-broken monitoring of bridge cable based on acoustic emission technique. In Proceedings of the 4th International Conference on Civil Engineering and Materials Science (ICCEMS 2019), Bangkok, Thailand, 17–19 May 2019; IOP Publishing Ltd.: Bristol, UK, 2019; Volume 652, p. 012065.
19. Djeddi, L.; Khelif, R.; Benmedakhene, S.; Favergeon, J. Reliability of acoustic emission as a technique to detect corrosion and stress corrosion cracking on prestressing steel strands. *Int. J. Electrochem. Sci.* **2013**, *8*, 8356–8370. [CrossRef]
20. Nair, A.; Cai, C.S. Acoustic emission monitoring of bridges: Review and case studies. *Eng. Struct.* **2010**, *32*, 1704–1714. [CrossRef]
21. Guohao, S.; Zhengxing, W.; Delian, K.; Mingqing, B.; Yang, Z.; Fengjing, X.; Jiazhen, P. Analysis on acoustic signal characteristics of the fatigue cracks in anchor structure of cable-stayed bridge tower. *Russ. J. Nondestr. Test* **2012**, *48*, 718–730. [CrossRef]
22. Kharrat, M.; Gaillet, L. Non-destructive evaluation of anchorage zones by ultrasonics techniques. *Ultrasonics* **2015**, *61*, 52–61. [CrossRef] [PubMed]
23. Xu, J.; Wu, X.; Sun, P. Detecting broken-wire flaws at multiple locations in the same wire of prestressing strands using guided waves. *Ultrasonics* **2013**, *53*, 150–156. [CrossRef]
24. Chen, X.; Zhu, J.; Lin, Y. Attenuation characteristics of low frequency longitudinal guided waves generated by magnetostrictive transducers in bridge cables. *Mech. Syst. Signal Proc.* **2022**, *164*, 108296. [CrossRef]
25. Zhang, Z.; Xu, J.; Guo, Z. A longitudinal mode guided wave transducer with the ring permanent biased magnet based on magnetostrictive effect for large diameter bridge cables. *IEEE Sens. J.* **2021**, *21*, 18544–18553. [CrossRef]
26. Park, S.; Kim, J.W.; Lee, C.; Lee, J.J. Magnetic flux leakage sensing-based steel cable NDE technique. *Shock Vib.* **2014**, *2014*, 929341. [CrossRef]
27. Zhang, Q.; Xin, R. The Defect-length effect in corrosion detection with magnetic method for bridge cables. *Front. Struct. Civ. Eng.* **2018**, *12*, 662–671. [CrossRef]
28. Ni, Y.; Zhang, Q.; Xin, R. Magnetic flux detection and identification of bridge cable metal area loss damage. *Measurement* **2021**, *167*, 108443. [CrossRef]
29. Xu, F.; Wang, X.; Wu, H. Inspection method of cable-stayed bridge using magnetic flux leakage detection: Principle, sensor design, and signal processing. *J. Mech. Sci. Technol.* **2012**, *26*, 661–669. [CrossRef]
30. Zhang, D.; Zhang, E.; Pan, S. A new signal processing method for the nondestructive testing of a steel wire rope using a small device. *NDT E Int.* **2020**, *114*, 102299. [CrossRef]
31. Xu, K.; Qiu, X.; Tian, X. Theoretical Investigation of Metal Magnetic Memory Testing Technique for Detection of Magnetic Flux Leakage Signals from Buried Defect. *Nondestruct. Test. Eval.* **2018**, *33*, 45–55. [CrossRef]
32. Qu, Y.; Zhou, J.; Liu, R.; Liao, L.; Zhao, Q. Research on the Detection of the Broken Wire Damage of a Cable in the Circumferential Directions Based on Self-Magnetic Flux Leakage. *KSCE J. Civ. Eng.* **2021**, *25*, 879–890. [CrossRef]
33. Xia, R.; Zhang, H.; Zhou, J.; Liao, L.; Zhang, Z.; Yang, F. Probability Evaluation Method of Cable Corrosion Degree Based on Self-Magnetic Flux Leakage. *J. Magn. Magn. Mater.* **2021**, *522*, 167544. [CrossRef]
34. Xia, R.; Zhang, H.; Zhou, J.; Liao, L.; Yang, W.; Li, Y. Corrosion Non-Destructive Testing of Loaded Steel Strand Based on Self-Magnetic Flux Leakage Effect. *Nondestruct. Test. Eval.* **2022**, *37*, 56–70. [CrossRef]
35. Nguyen, K.D.; Kim, J.T.; Park, Y.H. Multiscale Structural Health Monitoring of Cable-Anchorage System Using Piezoelectric PZT Sensors. *Int. J. Distrib. Sens. Netw.* **2013**, *9*, 254785. [CrossRef]
36. Zhang, X.; Zhang, L.; Liu, L.; Huo, L. Prestress Monitoring of a Steel Strand in an Anchorage Connection Using Piezoceramic Transducers and Time Reversal Method. *Sensors* **2018**, *18*, 4018. [CrossRef]
37. Ho, H.N.; Kim, K.D.; Park, Y.S.; Lee, J.J. An Efficient Image-Based Damage Detection for Cable Surface in Cable-Stayed Bridges. *NDT E Int.* **2013**, *58*, 18–23. [CrossRef]
38. Hou, S.; Dong, B.; Wang, H.; Wu, G. Inspection of Surface Defects on Stay Cables Using a Robot and Transfer Learning. *Autom. Constr.* **2020**, *119*, 103382. [CrossRef]
39. Li, X.; Gao, C.; Guo, Y.; He, F.; Shao, Y. Cable Surface Damage Detection in Cable-Stayed Bridges Using Optical Techniques and Image Mosaicking. *Opt. Laser Technol.* **2019**, *110*, 36–43. [CrossRef]
40. Han, L.; Li, W.; Bjorhovde, R. Developments and advanced applications of concrete-filled steel tubular (CFST) structures: Members. *J. Constr. Steel Res.* **2014**, *100*, 211–228. [CrossRef]
41. Chen, B.; Wang, T. Overview of concrete filled steel tube arch bridges in china. *Pract. Period. Struct. Des. Constr.* **2009**, *14*, 70–80. [CrossRef]
42. Iyer, S.; Sinha, S.K.; Tittmann, B.R.; Pedrick, M.K. Ultrasonic signal processing methods for detection of defects in concrete pipes. *Autom. Constr.* **2012**, *22*, 135–148. [CrossRef]
43. Hola, J.; Sadowski, L.; Schabowicz, K. Nondestructive identification of delaminations in concrete floor toppings with acoustic methods. *Autom. Constr.* **2011**, *20*, 799–807. [CrossRef]

44. Ding, R. Research on fiber sensing of health monitoring for steel tube-confined concrete arch bridge. *Chin. Civil. Eng. J.* **2005**, *38*, 69–147. (In Chinese)
45. Yan, Q.; Cheng, X.; Ding, R. Application of distributed optical technique in sensing interface disengaging and cracks of steel tube-confined concrete. In Proceedings of the 2011 International Conference on Electric Technology and Civil Engineering (ICETCE), Lushan, China, 22–24 April 2011; pp. 122–126.
46. Clark, M.R.; McCann, D.M.; Forde, M.C. Application of infrared thermography to the non-destructive testing of concrete and masonry bridges. *NDT E. Int.* **2003**, *36*, 265–275. [CrossRef]
47. Zhang, H.; Yu, Q.; Lu, Y. Application study of quality testing of arch-rib concrete of concrete filled steel tube arch bridge by ultrasonic transmission method. *Chin. Civil Eng. J.* **2004**, *37*, 50–53. (In Chinese)
48. Liu, Y.; Zhang, Y.; Zou, Z. Study of ultrasonic detection and evaluation for the deficiency of concrete-filled steel tube arch bridge. *J. Beijing Jiaotong Univ.* **2004**, *28*, 54–57. (In Chinese)
49. Dong, W.; Wu, Z.; Zhou, X.; Tan, Y. Experimental studies on void detection in concrete-filled steel tubes using ultrasound. *Constr. Build. Mater.* **2016**, *128*, 154–162. [CrossRef]
50. Callejas, A.; Palma, R.; Hernández-Figueirido, D.; Rus, G. Damage detection using ultrasonic techniques in concrete-filled steel tubes (CFSTs) columns. *Sensors* **2022**, *22*, 4400. [CrossRef] [PubMed]
51. Liu, H.; Xia, H.; Zhuang, M.; Long, Z.; Liu, C.; Cui, J.; Xu, B.; Hu, Q.; Liu, Q.H. Reverse Time Migration of Acoustic Waves for Imaging Based Defects Detection for Concrete and CFST Structures. *Mech. Syst. Signal Process.* **2019**, *117*, 210–220. [CrossRef]
52. Liu, H.; Chen, Z.; Liu, Y.; Chen, Y.; Du, Y.; Zhou, F. Interfacial debonding detection for cfst structures using an ultrasonic phased array: Application to the Shenzhen SEG building. *Mech. Syst. Signal Process.* **2023**, *192*, 110214. [CrossRef]
53. Büyüköztürk, O. Imaging of concrete structures. *NDT E Int.* **1998**, *31*, 233–243. [CrossRef]
54. Sansalone, M.; Carino, N.J.; Hsu, N.N. Flaws detection in concrete by frequency spectrum analysis of impact-echo waveforms. *J. Res. Natl. Bur. Stand.* **1987**, *7*, 279–290. [CrossRef]
55. Zhang, D.; Wang, Y. Study of impact-echo method detection in arch bridge of concrete-filled steel tube. *Chin. J. Eng. Geophys.* **2009**, *6*, 364–367. (In Chinese)
56. Liu, Y.; Liu, Z.; Lai, S.; Luo, L.; Dai, J. Debonding detection in the grouted joints of precast concrete shear walls using impact-echo method. *J. Nondestruct. Eval.* **2021**, *40*, 50. [CrossRef]
57. Yang, C.; Yu, Q. Placement and Size-Oriented Heat Dissipation Optimization for Antenna Module in Space Solar Power Satellite Based on Interval Dimension-Wise Method. *Aerosp. Sci. Technol.* **2023**, *134*, 108155. [CrossRef]
58. Yang, C.; Xia, Y. Interval Uncertainty-Oriented Optimal Control Method for Spacecraft Attitude Control. *IEEE Trans. Aerosp. Electron. Syst.* **2023**, 1–13. [CrossRef]
59. Chen, D.; Montano, V.; Huo, L.; Fan, S.; Song, G. Detection of subsurface voids in concrete-filled steel tubular (CFST) structure using percussion approach. *Constr. Build. Mater.* **2020**, *262*, 119761. [CrossRef]
60. Chen, H.; Nie, X.; Gan, S.; Zhao, Y.; Qiu, H. Interfacial imperfection detection for steel-concrete composite structures using ndt techniques: A state-of-the-art review. *Eng. Struct.* **2021**, *245*, 112778. [CrossRef]
61. Ansari, F. Practical implementation of optical fiber sensors in civil structural health monitoring. *J. Intell. Mater. Syst. Struct.* **2007**, *18*, 879–889. [CrossRef]
62. Gong, S.; Feng, X.; Zhang, G. A thermal-driven method based on brillouin fiber-optic sensors for the quantitative identification of subsurface cavities in concrete-filled steel tube structures. *J. Civ. Struct. Health Monit.* **2021**, *11*, 521–536. [CrossRef]
63. Wang, W.; Wang, G.; Wei, D.; Yang, H. Experimental study on detection of compactness of steel pipe concrete by rubber heating belt. *China Concr. Cem. Prod.* **2018**, 74–77. (In Chinese) [CrossRef]
64. Guo, X.; Yan, H. Analysis of influence factors for CFST arch bridge void based on eddy current thermal imaging. *Int. J. Robot. Autom.* **2021**, 36. [CrossRef]
65. Jiang, H.; Chen, L. Research status and development trend of pulsed infrared nondestructive testing technology. *Infrared Technol.* **2018**, *40*, 946–951+965. (In Chinese)
66. Zhang, S.; Tan, S.; Xu, L.; Chen, L. Thermoimage enhancement method for hollowing detection of steel tube concrete based on CLAHE. *J. Xihua Univ. Nat. Sci. Ed.* **2019**, *38*, 107–112. (In Chinese)
67. Zheng, D.; Tan, S. Research on internal defect detection of concrete based on infrared image enhancement algorithm. *J. Chongqing Jiaotong Univ. Nat. Sci. Ed.* **2021**, *40*, 114–117+127. (In Chinese)
68. Xu, R.; Jiang, D.; Lu, X. Research on the application of the infrared thermal image method in detection of concrete density of concrete-filled steel tube. *Appl. Mech. Mater.* **2012**, *166*, 998–1001. [CrossRef]
69. Sarhosis, V.; Santis, S.D.; de Felice, G. A Review of Experimental Investigations and Assessment Methods for Masonry Arch Bridges. *Struct. Infrastruct. E* **2016**, *12*, 1439–1464.
70. Gholizadeh, S. A Review of Non-Destructive Testing Methods of Composite Materials. *Procedia Struct. Integr.* **2016**, *1*, 50–57. [CrossRef]
71. Shang, R.; Zeng, B.; Rong, H.; Xu, Q.; Xu, M.; Xu, X. Research on Standardized Method of Stress Release Method for Measuring the Stress of Concrete. *Ind. Constr.* **2022**, *52*, 151–156. (In Chinese)
72. Pan, L. Example for calculating actual internal forces of concrete members by Hole Method of Reinforcement. *Build. Struct.* **2019**, *49*, 57–60. (In Chinese)

73. Ju, H.; Lin, C.; Zhang, J.; Liu, Z. Residual Stress Simulation and Measurement of Fe-Mn-Si Shape Memory Alloy Coating. *Infrared Laser Eng.* **2017**, *46*, 1017009. (In Chinese)
74. Bobzin, K.; Wietheger, W.; Knoch, M.A.; Schacht, A.; Reisgen, U.; Sharma, R.; Oster, L. Comparison of Residual Stress Measurements Conducted by X-Ray Stress Analysis and Incremental Hole Drilling Method. *J. Therm. Spray Tech.* **2020**, *29*, 1218–1228. [CrossRef]
75. Mohamed Karim, H.; Lamine, H.; Nadir, M. Assessment of Non-Uniform Residual Stress Field of the Thermal Sprayed Stainless Steel Coatings on Aluminium Substrates by the Integral Hole Drilling Method. *Proc. Inst. Mech. Eng. Part C J. Mech. Eng. Sci.* **2022**, *236*, 10701–10712. [CrossRef]
76. Razumovskii, I.A.; Usov, S.M. Development of the Hole-Drilling Method as Applied to the Study of Inhomogeneous Residual Stress Fields. *J. Mach. Manuf. Reliab.* **2021**, *50*, 727–734. [CrossRef]
77. Keil, S. Experimental determination of residual stresses with the ring-core method and an on-line measuring system. *Exp. Tech.* **2008**, *16*, 17–24. [CrossRef]
78. Chen, Z.; Sun, G.; Zhao, Y. Extension of Applicable Range of Measuring Residual Stress by Ring-Core Method. *Mater. Mech. Eng.* **2015**, *39*, 47–50+54. (In Chinese)
79. Li, K.; Ren, W. Application of Minature Ring-Core and Interferometric Strain/Slope Rosette to Determine Residual Stress Distribution With Depth—Part I: Theories. *J. Appl. Mech.* **2007**, *74*, 298–306. [CrossRef]
80. Hu, Z.; Xie, H.; Lu, J.; Zhu, J.; Wang, H. Residual Stresses Measurement by Using Ring-Core Method and 3D Digital Image Correlation Technique. *Meas. Sci. Technol.* **2013**, *24*, 085604. [CrossRef]
81. Dang, N.; Ku, W.; Wang, Z.; Lin, C.; Chen, T.; Lin, M. Incremental FIB-DIC Ring-Core Methods for the Residual Stress Measurement of Bilayer Thin Films. *Exp. Mech.* **2022**, *62*, 1489–1499. [CrossRef]
82. Sanginabadi, K.; Yazdani, A.; Mostofinejad, D.; Czaderski, C. RC Members Externally Strengthened with FRP Composites by Grooving Methods Including EBROG and EBRIG: A State-of-the-Art Review. *Constr. Build. Mater.* **2022**, *324*, 126662. [CrossRef]
83. Zhu, R.; Yin, Y.; Xie, H.; Liu, Y. On the Micro-Residlual Stress Measurement of Shot PeenedNickel-Based Alloy Material by using Slot-Milling Method. *J. Exp. Mech.* **2017**, *32*, 145–151. (In Chinese)
84. Shomali, A.; Mostofinejad, D.; Esfahani, M.R. Experimental and Numerical Investigation of Shear Performance of RC Beams Strengthened with FRP Using Grooving Method. *J. Build. Eng.* **2020**, *31*, 101409. [CrossRef]
85. Yan, Y.; Sun, Y.; He, L.; Zheng, L. Concrete Beam Stress Test Based on Grooving Method. *J. Chongqing Jiaotong Univ. (Nat. Sci.)* **2022**, *41*, 71–75+94. (In Chinese)
86. Dwivedi, S.K.; Vishwakarma, M.; Soni, A. Advances and Researches on Non Destructive Testing: A Review. *Mater. Today Proc.* **2018**, *5*, 3690–3698. [CrossRef]
87. Huang, Y.H.; Liu, L.; Sham, F.C.; Chan, Y.S.; Ng, S.P. Optical Strain Gauge vs. Traditional Strain Gauges for Concrete Elasticity Modulus Determination. *Optik* **2010**, *121*, 1635–1641. [CrossRef]
88. Zhao, Y.; Liu, Y.; Li, Y.; Hao, Q. Development and Application of Resistance Strain Force Sensors. *Sensors* **2020**, *20*, 5826. [CrossRef]
89. Kovačič, B.; Kamnik, R.; Štrukelj, A.; Vatin, N. Processing of Signals Produced by Strain Gauges in Testing Measurements of the Bridges. *Procedia Eng.* **2015**, *117*, 795–801. [CrossRef]
90. Turan, M.E.; Aydin, F.; Sun, Y.; Cetin, M. Residual Stress Measurement by Strain Gauge and X-Ray Diffraction Method in Different Shaped Rails. *Eng. Fail. Anal.* **2019**, *96*, 525–529. [CrossRef]
91. Ma, Z.; Chung, J.; Liu, P.; Sohn, H. Bridge Displacement Estimation by Fusing Accelerometer and Strain Gauge Measurements. *Struct. Control Health Monit.* **2021**, *28*, e2733. [CrossRef]
92. Takebayashi, S.; Kunieda, T.; Yoshinaga, N.; Ushioda, K.; Ogata, S. Comparison of the Dislocation Density in Martensitic Steels Evaluated by Some X-Ray Diffraction Methods. *ISIJ Int.* **2010**, *50*, 875–882. [CrossRef]
93. Macherauch, E. X-Ray Stress Analysis: Paper Covers Some Rather Important Developments during the Last Decade, Including New Experimental Results and Theoretical Aspects of X-Ray Stress Analysis. *Exp. Mech.* **1966**, *6*, 140–153. [CrossRef]
94. Monin, V.I.; Gurova, T.; Castello, X.; Estefen, S.F. Analysis of residual stress state in welded steel plates by x-ray diffraction method. *Rev. Adv. Mater. Sci.* **2009**, *20*, 172–175.
95. Epp, J. X-Ray Diffraction (XRD) Techniques for Materials Characterization. In *Materials Characterization Using Nondestructive Evaluation (NDE) Methods*; Elsevier: Amsterdam, The Netherlands, 2016; pp. 81–124.
96. Morin, L.; Braham, C.; Tajdary, P.; Seddik, R.; Gonzalez, G. Reconstruction of Heterogeneous Surface Residual-Stresses in Metallic Materials from X-Ray Diffraction Measurements. *Mech. Mater.* **2021**, *158*, 103882. [CrossRef]
97. Shi, P.; Su, S.; Chen, Z. Overview of Researches on the Nondestructive Testing Method of Metal Magnetic Memory: Status and Challenges. *J. Nondestruct. Eval.* **2020**, *39*, 43. [CrossRef]
98. Bao, S.; Jin, P.; Zhao, Z.; Fu, M. A Review of the Metal Magnetic Memory Method. *J. Nondestruct. Eval.* **2020**, *39*, 11. [CrossRef]
99. Dubov, A.; Dubov, A.; Kolokolnikov, S. Application of the Metal Magnetic Memory Method for Detection of Defects at the Initial Stage of Their Development for Prevention of Failures of Power Engineering Welded Steel Structures and Steam Turbine Parts. *Weld. World* **2014**, *58*, 225–236. [CrossRef]
100. Huang, H.; Jiang, S.; Wang, Y.; Zhang, L.; Liu, Z. Characterization of Spontaneous Magnetic Signals Induced by Cyclic Tensile Stress in Crack Propagation Stage. *J. Magn. Magn. Mater.* **2014**, *365*, 70–75. [CrossRef]
101. Chen, C.; Zeng, S.; Su, L. Strain Energy Based Method for Metal Magnetic Memory Effect of Tensile Tested Structures. *J. Nondestruct. Eval.* **2019**, *38*, 36. [CrossRef]

102. Tong, K.; Zhou, J.; Zhao, R.; Hu, W.; Qu, Y.; Cheng, C. Experimental Study on Rebar Stress Measurement Based on Force-Magnetic Coupling under Excited Magnetic Field. *Measurement* **2022**, *189*, 110620. [CrossRef]
103. Tong, K.; Zhou, J.; Zhao, R.; Ying, H.; Zhang, S. Quantitative Measurement of Stress in Steel Bars under Repetitive Tensile Load Based on Force-Magnetic Coupling Effect. *Measurement* **2022**, *202*, 111820. [CrossRef]
104. Zhang, W.; Qiu, Z.; Yu, X.; Sun, H. Feasibility Analyses of Improving Magnetic Memory Testing Sensibility by Strengthening Magnetic Excitation Field. *China Mech. Eng.* **2015**, *26*, 3375–3378.
105. Leng, J.; Xu, M.; Zhou, G.; Wu, Z. Effect of Initial Remanent States on the Variation of Magnetic Memory Signals. *NDT E Int.* **2012**, *52*, 23–27. [CrossRef]
106. Tong, K.; Zhou, J.; Ma, X.; Ying, H.; Zhao, R. Investigation of the Effect of Initial Magnetization State on the Force-Magnetic Coupling Effect of Rebars. *J. Magn. Magn. Mater.* **2023**, *569*, 170382. [CrossRef]
107. Hu, B.; Li, L.; Chen, X.; Zhong, L. Study on the Influencing Factors of Magnetic Memory Method. *Int. J. Appl. Electrom.* **2010**, *33*, 1351–1357. [CrossRef]
108. Liu, L.; Chen, W.; Zhang, P.; Tan, A. Effects of external magnetic field interference on tensile stress measurement with magnetic memory technology. *Chin. J. Sci. Instrum.* **2012**, *33*, 2194.
109. Acevedo, R.; Sedlak, P.; Kolman, R.; Fredel, M. Residual Stress Analysis of Additive Manufacturing of Metallic Parts Using Ultrasonic Waves: State of the Art Review. *J. Mater. Res. Technol.* **2020**, *9*, 9457–9477. [CrossRef]
110. Pilarski, A.; Rose, J.L. A Transverse-wave Ultrasonic Oblique-incidence Technique for Interfacial Weakness Detection in Adhesive Bonds. *J. Appl. Phys.* **1988**, *63*, 300–307. [CrossRef]
111. Chaki, S.; Corneloup, G.; Lillamand, I.; Walaszek, H. Combination of Longitudinal and Transverse Ultrasonic Waves for In Situ Control of the Tightening of Bolts. *J. Press. Vessel Technol.* **2007**, *129*, 383–390. [CrossRef]
112. Liu, H.; Li, Y.; Li, T.; Zhang, X.; Liu, Y.; Liu, K.; Wang, Y. Influence Factors Analysis and Accuracy Improvement for Stress Measurement Using Ultrasonic Longitudinal Critically Refracted (LCR) Wave. *Appl. Acoust.* **2018**, *141*, 178–187. [CrossRef]
113. Eremeyev, V.A.; Rosi, G.; Naili, S. Transverse Surface Waves on a Cylindrical Surface with Coating. *Int. J. Eng. Sci.* **2020**, *147*, 103188. [CrossRef]
114. Balonis, M.; Sant, G.; Burkan Isgor, O. Mitigating Steel Corrosion in Reinforced Concrete Using Functional Coatings, Corrosion Inhibitors, and Atomistic Simulations. *Cement Concrete Comp.* **2019**, *101*, 15–23. [CrossRef]
115. Goyal, A.; Ganjian, E.; Pouya, H.S.; Tyrer, M. Inhibitor Efficiency of Migratory Corrosion Inhibitors to Reduce Corrosion in Reinforced Concrete Exposed to High Chloride Environment. *Constr. Build. Mater.* **2021**, *303*, 124461. [CrossRef]
116. Kim, B.; Cho, S. Image-based Concrete Crack Assessment Using Mask and Region-based Convolutional Neural Network. *Struct. Control Health Monit.* **2019**, *26*, e2381. [CrossRef]
117. James, A.; Bazarchi, E.; Chiniforush, A.A.; Panjebashi Aghdam, P.; Hosseini, M.R.; Akbarnezhad, A.; Martek, I.; Ghodoosi, F. Rebar Corrosion Detection, Protection, and Rehabilitation of Reinforced Concrete Structures in Coastal Environments: A Review. *Constr. Build. Mater.* **2019**, *224*, 1026–1039. [CrossRef]
118. Rodrigues, R.; Gaboreau, S.; Gance, J.; Ignatiadis, I.; Betelu, S. Reinforced Concrete Structures: A Review of Corrosion Mechanisms and Advances in Electrical Methods for Corrosion Monitoring. *Constr. Build. Mater.* **2021**, *269*, 121240. [CrossRef]
119. Tešić, K.; Baričević, A.; Serdar, M. Non-Destructive Corrosion Inspection of Reinforced Concrete Using Ground-Penetrating Radar: A Review. *Materials* **2021**, *14*, 975. [CrossRef]
120. Amalia, Z.; Qiao, D.; Nakamura, H.; Miura, T.; Yamamoto, Y. Development of Simulation Method of Concrete Cracking Behavior and Corrosion Products Movement Due to Rebar Corrosion. *Constr. Build. Mater.* **2018**, *190*, 560–572. [CrossRef]
121. Alonso, C.; Andrade, C.; Rodriguez, J.; Diez, J.M. Factors Controlling Cracking of Concrete Affected by Reinforcement Corrosion. *Mater. Struct.* **1998**, *31*, 435–441. [CrossRef]
122. Liang, Y.; Wang, L. Prediction of Corrosion-Induced Cracking of Concrete Cover: A Critical Review for Thick-Walled Cylinder Models. *Ocean Eng.* **2020**, *213*, 107688. [CrossRef]
123. Di, X.; Zhou, Y. Durability design methods for concrete structures. *Archit. Sci.* **1997**, *1*, 16–20. (In Chinese)
124. Hui, Y.; Li, R.; Lin, Z.; Quan, M. Experimental study on the performance of steel bars in basic concrete components before and after corrosion. *Ind. Constr.* **1997**, *6*, 15–19+58. (In Chinese)
125. Niu, D.; Zhai, B.; Wang, K.; Di, X.; Wang, Q. Analysis of bearing capacity of corroded reinforced concrete beams. *Build. Struct.* **1999**, *29*, 23–25. (In Chinese) [CrossRef]
126. Wang, S.; Zhang, W.; Zhang, Y. Research on Predicting Steel Bar Section Loss from Longitudinal Crack Width of Concret. In Proceedings of the Engineering Safety and Durability—Proceedings of the 9th Annual Conference of the Chinese Society of Civil Engineering, Shanghai, China, 30 June–5 July 2019; pp. 361–364. (In Chinese).
127. Wang, Q. *Durability Evaluation Standard for Concrete Structures Shaanxi Province*; Xi'an University of Architecture and Technology: Xi'an, China, 2005. (In Chinese)
128. Zhang, J.; Mao, Y.; Zhang, J. Comparative analysis of steel bar corrosion prediction model experiments. *Highw. Transp. Technol. (Appl. Technol. Ed.)* **2016**, *12*, 223–225. (In Chinese)
129. Molina, F.J.; Alonso, C.; Andrade, C. Cover Cracking as a Function of Rebar Corrosion: Part 2—Numerical Model. *Mater. Struct.* **1993**, *26*, 532–548. [CrossRef]
130. Hu, J.; Zhang, S.; Chen, E.; Li, W. A Review on Corrosion Detection and Protection of Existing Reinforced Concrete (RC) Structures. *Constr. Build. Mater.* **2022**, *325*, 126718. [CrossRef]

131. Mei, K.; He, Z.; Yi, B.; Lin, X.; Wang, J.; Wang, H.; Liu, J. Study on Electrochemical Characteristics of Reinforced Concrete Corrosion under the Action of Carbonation and Chloride. *Case. Stud. Constr. Mat.* **2022**, *17*, e01351. [CrossRef]
132. Amiri, A.S.; Erdogmus, E.; Richter-Egger, D. A Comparison between Ultrasonic Guided Wave Leakage and Half-Cell Potential Methods in Detection of Corrosion in Reinforced Concrete Decks. *Signals* **2021**, *2*, 413–433. [CrossRef]
133. Adriman, R.; Bin, M.; Ibrahim, I.; Huzni, S.; Fonna, S.; Ariffin, A.K. Improving Half-Cell Potential Survey through Computational Inverse Analysis for Quantitative Corrosion Profiling. *Case. Stud. Constr. Mat.* **2022**, *16*, e00854. [CrossRef]
134. Almashakbeh, Y.; Saleh, E.; Al-Akhras, N.M. Evaluation of Half-Cell Potential Measurements for Reinforced Concrete Corrosion. *Coatings* **2022**, *12*, 975. [CrossRef]
135. Fan, L.; Bao, Y. Review of Fiber Optic Sensors for Corrosion Monitoring in Reinforced Concrete. *Cement Concrete Comp.* **2021**, *120*, 104029. [CrossRef]
136. Zhao, B.; Yao, K.; Wu, L.; Li, X.; Wang, Y. Application of Metal Magnetic Memory Testing Technology to the Detection of Stress Corrosion Defect. *Appl. Sci.* **2020**, *10*, 7083. [CrossRef]
137. Zhou, J.; Qiu, J.; Zhou, Y.; Zhou, Y.; Xia, R. Experimental Study on Residual Bending Strength of Corroded Reinforced Concrete Beam Based on Micromagnetic Sensor. *Sensors* **2018**, *18*, 2635. [CrossRef]
138. Qiu, J.; Zhang, H.; Zhou, J.; Ma, H.; Liao, L. Experimental Analysis of the Correlation between Bending Strength and SMFL of Corroded RC Beams. *Constr. Build. Mater.* **2019**, *214*, 594–605. [CrossRef]
139. Xia, R.; Zhou, J.; Zhang, H.; Liao, L.; Zhao, R.; Zhang, Z. Quantitative Study on Corrosion of Steel Strands Based on Self-Magnetic Flux Leakage. *Sensors* **2018**, *18*, 1396. [CrossRef]
140. Xia, R.; Zhou, J.; Zhang, H.; Zhou, D.; Zhang, Z. Experimental Study on Corrosion of Unstressed Steel Strand Based on Metal Magnetic Memory. *KSCE J. Civ. Eng.* **2019**, *23*, 1320–1329. [CrossRef]
141. Su, S.; Ma, X.; Wang, W.; Yang, Y.; Hu, J. Quantitative Evaluation of Cumulative Plastic Damage for Ferromagnetic Steel under Low Cycle Fatigue Based on Magnetic Memory Method. *Strain* **2021**, *57*, e12379. [CrossRef]
142. Yang, Y.; Ma, X.; Su, S.; Wang, W. Study on Corrosion Damage Characterization and Tensile Strength Evaluation for Locally Corroded Bridge Steel via Metal Magnetic Memory Method. *Measurement* **2023**, *207*, 112406. [CrossRef]
143. Yang, C.; Liang, K.; Zhang, X.; Geng, X. Sensor Placement Algorithm for Structural Health Monitoring with Redundancy Elimination Model Based on Sub-Clustering Strategy. *Mech. Syst. Signal Process.* **2019**, *124*, 369–387. [CrossRef]
144. Yang, C.; Xia, Y. A Novel Two-Step Strategy of Non-Probabilistic Multi-Objective Optimization for Load-Dependent Sensor Placement with Interval Uncertainties. *Mech. Syst. Signal Process.* **2022**, *176*, 109173. [CrossRef]
145. An, Y.; Chatzi, E.; Sim, S.; Laflamme, S.; Blachowski, B.; Ou, J. Recent Progress and Future Trends on Damage Identification Methods for Bridge Structures. *Struct. Control Health Monit.* **2019**, *26*, e2416. [CrossRef]
146. Yang, C.; Ouyang, H. A Novel Load-Dependent Sensor Placement Method for Model Updating Based on Time-Dependent Reliability Optimization Considering Multi-Source Uncertainties. *Mech. Syst. Signal Process.* **2022**, *165*, 108386. [CrossRef]
147. Serra, M.; Festa, G.; Vassallo, M.; Zollo, A.; Quattrone, A.; Ceravolo, R. Damage Detection in Elastic Properties of Masonry Bridges Using Coda Wave Interferometry. Struct. *Control Health Monit.* **2017**, *24*, e1976. [CrossRef]
148. Emre Alpaslan, Z.K. Response Surface-Based Model Updating to Detect Damage on Reduced-Scale Masonry Arch Bridge. *Struct. Eng. Mech.* **2021**, *79*, 9–22.
149. Civera, M.; Calamai, G.; Zanotti Fragonara, L. System Identification via Fast Relaxed Vector Fitting for the Structural Health Monitoring of Masonry Bridges. *Structures* **2021**, *30*, 277–293. [CrossRef]
150. Civera, M.; Mugnaini, V.; Zanotti Fragonara, L. Machine Learning-based Automatic Operational Modal Analysis: A Structural Health Monitoring Application to Masonry Arch Bridges. *Struct. Control Health Monit.* **2022**, *29*, e3028. [CrossRef]
151. Conde, B.; Eguía, P.; Stavroulakis, G.E.; Granada, E. Parameter Identification for Damaged Condition Investigation on Masonry Arch Bridges Using a Bayesian Approach. *Eng. Struct.* **2018**, *172*, 275–284. [CrossRef]
152. Borlenghi, P.; Saisi, A.; Gentile, C. ND Testing and Establishing Models of a Multi-Span Masonry Arch Bridge. *J. Civ. Struct. Health Monit.* **2023**. [CrossRef]
153. Alexakis, H.; Liu, H.; DeJong, M.J. Damage Identification of Brick Masonry under Cyclic Loading Based on Acoustic Emissions. *Eng. Struct.* **2020**, *221*, 110945. [CrossRef]
154. Pepi, C.; Cavalagli, N.; Gusella, V.; Gioffrè, M. An Integrated Approach for the Numerical Modeling of Severely Damaged Historic Structures: Application to a Masonry Bridge. *Adv. Eng. Softw.* **2021**, *151*, 102935. [CrossRef]
155. Batar, O.S.; Tercan, E.; Emsen, E. Ayvalıkemer (Sillyon) Historical Masonry Arch Bridge: A Multidisciplinary Approach for Structural Assessment Using Point Cloud Data Obtained by Terrestrial Laser Scanning (TLS). *J. Civ. Struct. Health Monit.* **2021**, *11*, 1239–1252. [CrossRef]
156. Deng, Y.; Jia, Y.; Li, Y.; Li, A. Structural Parameter Identification of Ancient Stone Arch Bridge via Three-Dimensional Laser Ranger Scanning. *J. Perform. Constr. Facil.* **2022**, *36*, 04022041. [CrossRef]
157. Jara, J.M.; López, J.I.; Olmos, B.A.; Martínez, G. Effect of Seismic Source Type on the Expected Behavior of Historic Arch Bridges. *Int. J. Archit. Herit.* **2022**, *16*, 789–815. [CrossRef]
158. Kaya, A.; Adanur, S.; Bello, R.A.; Genç, A.F.; Okur, F.Y.; Sunca, F.; Günaydin, M.; Altunişik, A.C.; Sevim, B. Post-Earthquake Damage Assessments of Unreinforced Masonry (URM) Buildings by Shake Table Test and Numerical Visualization. *Eng. Fail. Anal.* **2023**, *143*, 106858. [CrossRef]

159. Gönen, S.; Soyöz, S. Reliability-Based Seismic Performance of Masonry Arch Bridges. *Struct. Infrastruct. Eng.* **2022**, *18*, 1658–1673. [CrossRef]
160. Aytulun, E.; Soyoz, S.; Karcioglu, E. System Identification and Seismic Performance Assessment of a Stone Arch Bridge. *J. Earthq. Eng.* **2022**, *26*, 723–743. [CrossRef]
161. Mu, H.; Zheng, Z.; Wu, X.; Su, C. Bayesian Network-Based Modal Frequency–Multiple Environmental Factors Pattern Recognition for the Xinguang Bridge Using Long-Term Monitoring Data. *J. Low Freq. Noise Vib. Act. Control* **2020**, *39*, 545–559. [CrossRef]
162. Anastasopoulos, D.; Maes, K.; De Roeck, G.; Lombaert, G.; Reynders, E.P.B. Influence of Frost and Local Stiffness Variations on the Strain Mode Shapes of a Steel Arch Bridge. *Eng. Struct.* **2022**, *273*, 115097. [CrossRef]
163. Anastasopoulos, D.; De Roeck, G.; Reynders, E.P.B. One-Year Operational Modal Analysis of a Steel Bridge from High-Resolution Macrostrain Monitoring: Influence of Temperature vs. Retrofitting. *Mech. Syst. Signal Process.* **2021**, *161*, 107951. [CrossRef]
164. Zhu, Q.; Wang, H.; Spencer, B.F. Investigation on the Mapping for Temperature-Induced Responses of a Long-Span Steel Truss Arch Bridge. *Struct. Infrastruct. Eng.* **2022**, 1–18. [CrossRef]
165. Teng, J.; Tang, D.; Hu, W.; Lu, W.; Feng, Z.; Ao, C.; Liao, M. Mechanism of the Effect of Temperature on Frequency Based on Long-Term Monitoring of an Arch Bridge. *Struct. Health Monit.* **2021**, *20*, 1716–1737. [CrossRef]
166. Sunca, F.; Ergün, M.; Altunişik, A.C.; Günaydin, M.; Okur, F.Y. Modal Identification and Fatigue Behavior of Eynel Steel Arch Highway Bridge with Calibrated Models. *J. Civ. Struct. Health Monit.* **2021**, *11*, 1337–1354. [CrossRef]
167. Chiaia, B.; Marasco, G.; Ventura, G.; Zannini Quirini, C. Customised Active Monitoring System for Structural Control and Maintenance Optimisation. *J. Civ. Struct. Health Monit.* **2020**, *10*, 267–282. [CrossRef]
168. Dammika, A.J.; Kawarai, K.; Yamaguchi, H.; Matsumoto, Y.; Yoshioka, T. Analytical Damping Evaluation Complementary to Experimental Structural Health Monitoring of Bridges. *J. Bridge Eng.* **2015**, *20*, 04014095. [CrossRef]
169. Tran, T.T.X.; Ozer, E. Automated and Model-Free Bridge Damage Indicators with Simultaneous Multiparameter Modal Anomaly Detection. *Sensors* **2020**, *20*, 4752. [CrossRef]
170. Whelan, M.; Salas Zamudio, N.; Kernicky, T. Structural Identification of a Tied Arch Bridge Using Parallel Genetic Algorithms and Ambient Vibration Monitoring with a Wireless Sensor Network. *J. Civ. Struct. Health Monit.* **2018**, *8*, 315–330. [CrossRef]
171. Jayasundara, N.; Thambiratnam, D.; Chan, T.; Nguyen, A. Vibration-Based Dual-Criteria Approach for Damage Detection in Arch Bridges. *Struct. Health Monit.* **2019**, *18*, 2004–2019. [CrossRef]
172. Jayasundara, N.; Thambiratnam, D.P.; Chan, T.H.T.; Nguyen, A. Damage Detection and Quantification in Deck Type Arch Bridges Using Vibration Based Methods and Artificial Neural Networks. *Eng. Fail. Anal.* **2020**, *109*, 104265. [CrossRef]
173. Jayasundara, N.; Thambiratnam, D.P.; Chan, T.H.T.; Nguyen, A. Locating and Quantifying Damage in Deck Type Arch Bridges Using Frequency Response Functions and Artificial Neural Networks. *Int. J. Struct. Stab. Dyn.* **2020**, *20*, 2042010. [CrossRef]
174. Delgadillo, R.M.; Tenelema, F.J.; Casas, J.R. Marginal Hilbert Spectrum and Instantaneous Phase Difference as Total Damage Indicators in Bridges under Operational Traffic Loads. *Struct. Infrastruct. Eng.* **2023**, *19*, 824–844. [CrossRef]
175. Kordestani, H.; Xiang, Y.; Ye, X.; Yun, C.; Shadabfar, M. Localization of Damaged Cable in a Tied-arch Bridge Using Arias Intensity of Seismic Acceleration Response. *Struct. Control Health Monit.* **2020**, *27*, e2491. [CrossRef]
176. Magalhães, F.; Cunha, Á. Explaining Operational Modal Analysis with Data from an Arch Bridge. *Mech. Syst. Signal Process.* **2011**, *25*, 1431–1450. [CrossRef]
177. Magalhães, F.; Cunha, A.; Caetano, E. Vibration Based Structural Health Monitoring of an Arch Bridge: From Automated OMA to Damage Detection. *Mech. Syst. Signal Process.* **2012**, *28*, 212–228. [CrossRef]
178. Ren, W.; Lin, Y.; Fang, S. Structural Damage Detection Based on Stochastic Subspace Identification and Statistical Pattern Recognition: I. Theory. *Smart Mater. Struct.* **2011**, *20*, 115009. [CrossRef]
179. Lin, Y.; Ren, W.; Fang, S. Structural Damage Detection Based on Stochastic Subspace Identification and Statistical Pattern Recognition: II. Experimental Validation under Varying Temperature. *Smart Mater. Struct.* **2011**, *20*, 115010. [CrossRef]
180. Comanducci, G.; Magalhães, F.; Ubertini, F.; Cunha, Á. On Vibration-Based Damage Detection by Multivariate Statistical Techniques: Application to a Long-Span Arch Bridge. *Struct. Health Monit.* **2016**, *15*, 505–524. [CrossRef]
181. Ferrari, R.; Froio, D.; Rizzi, E.; Gentile, C.; Chatzi, E.N. Model Updating of a Historic Concrete Bridge by Sensitivity- and Global Optimization-Based Latin Hypercube Sampling. *Eng. Struct.* **2019**, *179*, 139–160. [CrossRef]
182. Duan, Y.; Chen, Q.; Zhang, H.; Yun, C.; Wu, S.; Zhu, Q. CNN-Based Damage Identification Method of Tied-Arch Bridge Using Spatial-Spectral Information. *Smart Struct. Syst.* **2019**, *23*, 507–520.
183. Zhou, S.; Jiang, Y.; Li, X.; Wu, Q. Vibration-based damage identification of reinforced concrete arch bridges using KALMAN–ARMA–GARCH model. *Int. J. Robot. Autom.* **2021**, *36*. [CrossRef]
184. Qin, X.; Zhang, L.; Yang, M.; Luo, H.; Liao, M.; Ding, X. Mapping Surface Deformation and Thermal Dilation of Arch Bridges by Structure-Driven Multi-Temporal DInSAR Analysis. *Remote Sens. Environ.* **2018**, *216*, 71–90. [CrossRef]
185. Wang, W.; Su, M.; Wang, C. Static Deflection Difference-Based Damage Identification of Hanger in Arch Bridges. *KSCE J. Civ. Eng.* **2022**, *26*, 5096–5106. [CrossRef]
186. Li, S.; Ou, J.; Wang, J.; Gao, X.; Yang, C. Level 2 Safety Evaluation of Concrete-filled Steel Tubular Arch Bridges Incorporating Structural Health Monitoring and Inspection Information Based on China Bridge Standards. *Struct. Control Health Monit.* **2018**, *26*, e2303. [CrossRef]
187. Fu, C.; Jiang, S. A Hybrid Data-Fusion System by Integrating CFD and PNN for Structural Damage Identification. *Appl. Sci.* **2021**, *11*, 8272. [CrossRef]

188. Gui, C.; Lin, W.; Huang, Z.; Xin, G.; Xiao, J.; Yang, L. A Decision-Making Algorithm for Concrete-Filled Steel Tubular Arch Bridge Maintenance Based on Structural Health Monitoring. *Materials* **2022**, *15*, 6920. [CrossRef]
189. Yan, W.; Ren, W. Operational Modal Parameter Identification from Power Spectrum Density Transmissibility. *Comput. Aided Civ. Infrastruct. Eng.* **2012**, *27*, 202–217. [CrossRef]
190. Xiong, C.; Yu, L.; Niu, Y. Dynamic Parameter Identification of a Long-Span Arch Bridge Based on GNSS-RTK Combined with CEEMDAN-WP Analysis. *Appl. Sci.* **2019**, *9*, 1301. [CrossRef]
191. Li, J.; Hao, H.; Xia, Y.; Zhu, H.-P. Damage detection of shear connectors in bridge structures with transmissibility in frequency domain. *Int. J. Struct. Stab. Dyn.* **2014**, *14*, 1350061. [CrossRef]